Magnetic excitations in the site-centered stripe phase: Spin-wave theory of coupled three-leg ladders

Martin Greiter and Holger Schmidt

Institut für Theorie der Kondensierten Materie and DFG Center for Functional Nanostructures (CFN), KIT, Campus Süd, D-76128 Karlsruhe, Germany

(Received 3 November 2010; published 25 April 2011)

The success of models of coupled two-leg spin ladders in describing the magnetic excitation spectrum of $La_{2-x}Ba_xCuO_4$ had been interpreted previously as evidence for bond-centered stripes. In a recent article, however, we determined the magnetic coupling induced by the charge stripes between bond- or site-centered spin stripes modeled by two- or three-leg ladders, respectively. We found that only the site-centered models order, while the coupling in bond-centered models is insufficient to trigger the quantum phase transition into the magnetically ordered state. We further indicated excellent agreement of a fully consistent analysis of coupled three-leg ladders using a spin wave theory of bond with the experimental data. Here, we provide a full and detailed account of this analysis.

DOI: 10.1103/PhysRevB.83.144422 PACS number(s): 74.72.−h, 74.20.Mn, 75.10.−b, 75.25.−j

I. INTRODUCTION

Twenty years after the discovery, the mechanism of high-T_c superconductivity in the copper oxide materials is still considered one of the most important outstanding problem in contemporary physics.[1,2] The materials are described by mobile charge carriers (holes) doped into a quasi-two-dimensional spin 1/2 antiferromagnet.[3,4] Inelastic neutron scattering experiments have revealed a magnetic resonance peak[5,6] and, in some compounds, periodic modulations in the spin and charge density (stripes).[7–14] Tranquada *et al.*[15] found that the magnetic excitation spectrum of stripe ordered $La_{1.875}Ba_{0.125}CuO_4$ looks similar to disordered $YBa_2Cu_3O_{6+x}$[6] or $Bi_2Sr_2CaCu_2O_{8+\delta}$,[16] and observed that the data are consistent with bond-centered stripes modeled by two-leg ladders. This experiment is considered of key importance for the field, as it it may provide the decisive hint as to within which framework copper oxide superconductors may be understood.

With regard to such a framework, there is no consensus at present, but a fierce competition among different schools of thought. One of these schools[10,11,13,14] attributes the unusual properties of the doped, two-dimensional antiferromagnets to their propensity to form stripes, or their proximity to a quantum critical point (QCP) at which stripe order sets in. The resulting picture is highly appealing. Static stripes have been observed[9,12] only in certain compounds, most notably $La_{2-x}Sr_xCuO_4$ at a hole doping concentration $x = \frac{1}{8}$, and are known to suppress superconductivity. On the other hand, the mere existence of stripes would impose an effective one dimensionality, and hence provide a framework to formulate fractionally quantized excitations. This one dimensionality would be roughly consistent with an enormous body of experimental data on the cuprates, including the electron spectral functions seen in angle-resolved photoemission spectroscopy (ARPES). The charge carriers, the holons, would predominantly reside in the charge stripes, as they could maximize their kinetic energy in these antiferromagnetically disordered regions. In the spin stripes, by contrast, the antiferromagnetic exchange energy between the spins would be maximized, at the price of infringing on the mobility of the charge carriers. Most importantly, the spin stripes would impose a coupling between the charge stripes, which would yield an effective, pairwise confinement between the low-energy spinon and holon excitations residing predominantly in the charge stripes. The mechanism of confinement would be similar to that of coupled spin chains or spin ladders.[17–19] The holes would be described by spinon-holon bound states, and the dominant contribution to the magnetic response measured in Tranquada's as well as all other neutron scattering experiments would come from spinon-spinon bound states.

The similarity of the "hour-glass" spectrum shown in Fig. 4(b) of Tranquada *et al.*[15] (which is reproduced for comparison in Fig. 1(b)) with the "elephants trousers" observed by Bourges *et al.*[6] (which are reproduced for comparison in Fig. 2) provides the most striking evidence in favor of the picture advocated by this school, which attributes the anomalous properties of generic, disordered CuO superconductors to the formation of dynamic (rather than static) stripes, which fluctuate on time scales which are slow compared to the energy scales of most experimental probes. This picture is considered to receive additional support by Xu *et al.*,[20] who observed that the magnetic response of $La_{1.875}Ba_{0.125}CuO_4$ at higher energies is independent of temperature, while the stripe order melts at about $T_{st} \sim 54$ K. Measurements on "untwinned" samples of $YBa_2Cu_3O_{6.6}$, where one would expect the dynamical stripes to orient themselves along one of the axis, however, exhibit a strong anisotropy in the response only at energies below the resonance,[21] while the response is fourfold rotationally symmetric at higher energies.[22] We believe, however, that this only indicates that the formation of stripe correlations, be it static or dynamic, is a low energy phenomenon, while the high energy response probes itinerant antiferromagnets at length scales on which the stripes are essentially invisible.

An extremely appealing feature of the experiment by Tranquada *et al.*[15] is that it immediately suggests a model of ferromagnetically coupled two-leg ladders, as the upper part of the measured spectrum agrees strikingly well with the triplon (or spinon-spinon bound state) mode of isolated two-leg ladders (see Fig. 1(b)). The experiment hence appeared to point to bond-centered rather than site-centered stripes, (i.e., stripes as depicted in Fig. 3(a) rather than Fig. 3(b)), and thereby to resolve a long outstanding issue.

 ©2011 American Physical Society

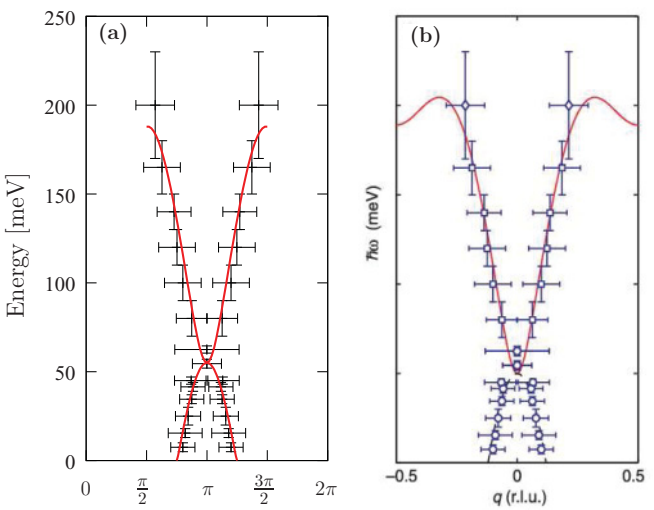

FIG. 1. (Color online) (a) Superpositions of cuts along (k_x, π) and (π, k_y) for the lowest mode $\omega(\boldsymbol{k})$ obtained with the bond operator spin wave theory of coupled three-leg ladders presented here (red line) superimposed with the experimental data obtained by inelastic neutron scattering by Tranquada *et al.*[15] (black). (b) The neutron data as originally presented, with a triplon dispersion of a two-leg ladder superimposed (red line) (reprinted by permission from Macmillian Publishers Ltd., Nature (London) **429**, 534 (2005).

This interpretation received support by theoretical studies.[23–25] Vojta and Ulbricht[23] used a bond operator formalism[26] similar to ours to study a spin-only model of stripes[27] of coupled two-leg ladders (as depicted in Fig. 3(a)) with $J_\parallel = J$, took into account a bond-boson renormalization[28] of J, and assumed a value J' for the ferromagnetic coupling between the ladders which is large enough to close the spin gap of the ladders, i.e., to induce long-range magnetic order. Within their approximations, a value of $J' = -0.06J$ is sufficient. This value is not consistent with previous studies,[29–31] but as no method to calculate or even estimate the true J' induced by charge stripes had been available, it did not seem a problem at the time. The spectrum they obtained agrees well with experimental data measured by Tranquada *et al.*,[15] and hence appeared to justify

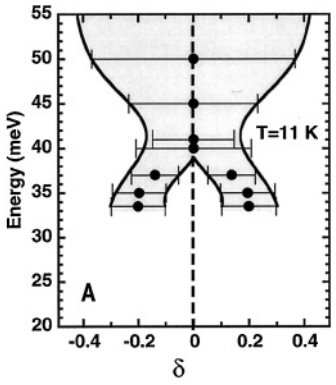

FIG. 2. Overall momentum dependence of the magnetic response of superconducting $YBa_2Cu_3O_{6.85}$ as reported by Bourges *et al.*[6] There is no stripe ordering in this compound (from Bourges *et al.*, Ref. 6; reprinted by permission from AAAS).

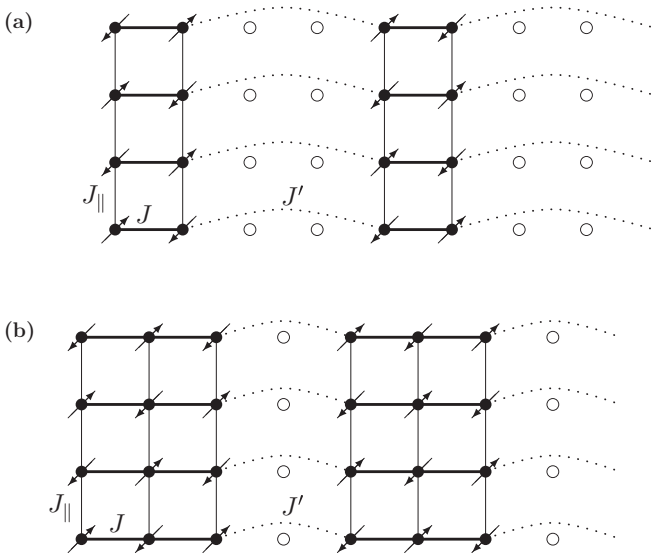

FIG. 3. Spin model for (a) bond-centered and (b) site-centered stripes in CuO superconductors.

their assumptions *a posteriori*. They concluded in favor of bond-centered stripes. This conclusion was independently strengthened by Uhrig, Schmidt, and Grüninger,[24] who used the method of continuous unitary transformations to study a model of ferromagnetically coupled two-leg ladders, and observed that the critical value of J'_c can be significantly reduced if a cyclic exchange term J_{cyc} on the ladders is included.[32] They likewise fine-tuned J' to the QCP where the gap closes and long-range magnetic order ensues, and reported good agreement with experiment.

On the other hand, Seibold and Lorenzana[33,34] calculated the magnetic response for a range of dopings within the time-dependent Gutzwiller approximation, and found good agreement with the measured data for both bond- and site-centered stripe models. Konik, Essler, and Tsvelik[35] studied a model of alternating coupled doped and undoped two-leg ladders, and found two distinct possible scenarios of magnetic ordering, which are both consistent with the experimental data.

In a recent article,[36] we investigated whether it is reasonable to assume that the ferromagnetic coupling J' induced by the charge stripe between the spin stripes modelled by two-leg ladders is sufficiently to induce long range order. There are several estimates for the critical value J'_c required if the coupling between isotropic ladders is antiferromagnetic in the literature. Gopalan, Rice, and Sigrist[29] find $J'_c \approx 0.25J$ in a simple mean-field treatment of bond bosons. Quantum Monte Carlo (QMC) calculations by Tworzydło *et al.*[30] yielded $J'_c = 0.30(2)J$, a value subsequently confirmed by Dalosto and Riera.[31] We redid the mean-field calculation of Gopalan *et al.*[29] for ferromagnetic (FM) couplings $J'_c < 0$, and found that within this approximation, the absolute value of J'_c is independent of the sign of the coupling. QMC calculations by Dalosto *et al.*,[31] however, indicate that the true value is at least $J_c = -0.4J$ (see Fig. 6(b) of their article). The physical reason why a significant coupling between the ladders is required to induce magnetic order is that the individual two-leg ladders possess a gap of order $\Delta \approx J/2$. As a cyclic exchange term

$J_{\rm cyc} \approx 0.25J$ reduces this gap by a factor of two,[32] we expected that $J_{\rm c}'$ would likewise be reduced by a factor of two. We hence concluded that a FM coupling of at least somewhere between $J_{\rm c}' = -0.2J$ and $-0.4J$ is required, depending on the strength of a possible cyclic exchange term.

The value we obtained for the ferromagnetic coupling induced by the charge stripes between the spin stripes through exact diagonalization of small clusters with and without charge stripes, however, is $J' = -0.05J$.[36] The details of this calculation are given in Appendix C. The coupling is hence insufficient to induce order in a model of coupled two-leg ladders describing bond-centered stripes. This does not imply that the stripes cannot be bond-centered, but rather implies that it is not sensible to describe bond-centered stripes through spin-only models of coupled two-leg ladders.

For a model of site-centered stripes described by antiferromagnetically coupled three-leg ladders, as shown in Fig. 3(b), the critical coupling required for long range order to set in is by contrast $J_{\rm c}' = 0$. The reason is simply that there is no need to close a gap, as the three-leg ladders are individually gapless.[17] A conventional spin wave analysis for such a spin-only model of three- and four-leg ladders was performed by Yao, Carlson, and Campbell,[37] who found that their approximation agrees reasonable well with the experimental data if they take $J' = 0.05J$ and $J' = -0.09J$ for coupled three- and four-leg ladders, respectively. The calculation we present in Appendix B, however, singles out $J' = 0.07J$ for the antiferromagnetic coupling between spin stripes modeled by three-leg ladders. In our previous work,[36] we announced that a fully consistent spin wave theory of bond operators representing the eight-dimensional Hilbert spaces on each rung of the three-leg ladders agrees perfectly with the experimental data if and only if the correct, calculated value $J' = 0.07J$ is used for the coupling.

In this context, one may ask whether it might be possible to obtain an equally valid description in terms of bond-centered stripes modelled by four-leg ladders. We believe the answer is no, as the width of the charge stripes in between the ladders would be zero, and one would have to assume that the antiferromagnetic coupling J between neighboring sites of the original t-J model, would turn into a weak ferromagnetic coupling between the four-leg ladders. There would be no foundation for such an assumption. Furthermore, since the four-leg ladders are gapped, just as the two-leg ladders are, one would need to fine tune this ferromagnetic coupling to exactly the point where the gap closes and magnetic order with $k = \pi \pm \pi/4$ emerges. So regardless of the agreement with the measured spectrum one might be able to obtain, we believe that a spin-only model of four-leg ladders would not constitute a valid theory.

In this paper, we provide a full and detailed account of our analysis of our spin-only model of coupled three-leg ladders. The paper is organized as follows. In Sec. II, we introduce a basis as well as a set of bosonic creation and annihilation operators for the three-site rungs of the ladders, in terms of which we write both the rung Hamiltonian and the spin operators on the individual sites. In Sec. III, we couple the rungs both along the ladders and across neighboring ladders, and self-consistently determine the fiducial state such that all the terms linear in a single creation or annihilation operator in the resulting Hamiltonian vanish. In Sec. IV, we rewrite this Hamiltonian in terms of momentum space operators, and expand it to bi-linear order in term of those. We then solve for the low energy spectrum using a multidimensional Bogoliubov transformation in Sec. V. In Sec. VI, we compare our results to the experimental data obtained by Tranquada *et al.*,[15] and investigate the dependence of the spectrum we obtain on the value of the interladder coupling J'. Finally, we present our conclusions in Sec. VII.

II. BASIS STATES FOR THREE-SITE RUNGS

To begin with, consider a single rung of a three-leg ladder, consisting of spins which are antiferromagnetically coupled with a coupling J we set to unity (see Fig. 4).

For later purposes, let us consider a rung belonging to sublattice $\mathcal{A}$, i.e., set-up conventions, the rungs belonging to sublattice $\mathcal{A}$ will inherit in the following sections. Denoting the SU(2) spin operators for the three spin $\frac{1}{2}$'s on the sites by $\boldsymbol{s}_1$,$\boldsymbol{s}_2$, and $\boldsymbol{s}_3$, the Hamiltonian for the rung reads

$$\hat{H}^{\mathcal{A}} = \hat{\boldsymbol{s}}_1\hat{\boldsymbol{s}}_2 + \hat{\boldsymbol{s}}_2\hat{\boldsymbol{s}}_3. \tag{1}$$

Diagonalization yields the following eigenvalues and eigenvectors:

$$E=-1 \begin{cases} |b_{-1/2}\rangle &= -\frac{1}{\sqrt{6}}\big(|\uparrow\downarrow\downarrow\rangle - 2|\downarrow\uparrow\downarrow\rangle + |\downarrow\downarrow\uparrow\rangle\big) \\ |b_{1/2}\rangle &= -\frac{1}{\sqrt{6}}\big(|\downarrow\uparrow\uparrow\rangle - 2|\uparrow\downarrow\uparrow\rangle + |\uparrow\uparrow\downarrow\rangle\big) \end{cases},$$

$$E=0 \begin{cases} |a_{-1/2}\rangle &= \frac{1}{\sqrt{2}}\big(|\uparrow\downarrow\downarrow\rangle - |\downarrow\downarrow\uparrow\rangle\big) \\ |a_{1/2}\rangle &= \frac{1}{\sqrt{2}}\big(|\downarrow\uparrow\uparrow\rangle - |\uparrow\uparrow\downarrow\rangle\big) \end{cases}, \tag{2}$$

$$E=\tfrac{1}{2} \begin{cases} |c_{-3/2}\rangle &= |\downarrow\downarrow\downarrow\rangle \\ |c_{-1/2}\rangle &= \frac{1}{\sqrt{3}}\big(|\downarrow\downarrow\uparrow\rangle + |\downarrow\uparrow\downarrow\rangle + |\uparrow\downarrow\downarrow\rangle\big) \\ |c_{1/2}\rangle &= \frac{1}{\sqrt{3}}\big(|\uparrow\uparrow\downarrow\rangle + |\uparrow\downarrow\uparrow\rangle + |\downarrow\uparrow\uparrow\rangle\big) \\ |c_{3/2}\rangle &= |\uparrow\uparrow\uparrow\rangle \end{cases}.$$

Note that the two states $|a_{-1/2}\rangle$ and $|a_{-1/2}\rangle$ are antisymmetric under spacial reflections interchanging sites 1 and 3 on the rung, while all other states are symmetric. This distinction will prove useful when expanding the Hamiltonian for the coupled ladders in Sec. IV below.

We denote the orthonormal basis formed by these eight states by

$$M = \{|b_{-1/2}\rangle,|b_{1/2}\rangle,|a_{-1/2}\rangle,|a_{1/2}\rangle, |c_{-3/2}\rangle,|c_{-1/2}\rangle,|c_{1/2}\rangle,|c_{3/2}\rangle\}. \tag{3}$$

In this basis, the Hamiltonian matrix is trivially given by

$$\begin{aligned}\hat{H}^{\mathcal{A}} = &-\big(|b_{-1/2}\rangle\langle b_{-1/2}| + |b_{1/2}\rangle\langle b_{1/2}|\big) \\ &+ \tfrac{1}{2}\big(|c_{-3/2}\rangle\langle c_{-3/2}| + |c_{-1/2}\rangle\langle c_{-1/2}| \\ &+ |c_{-1/2}\rangle\langle c_{-1/2}| + |c_{3/2}\rangle\langle c_{3/2}|\big).\end{aligned} \tag{4}$$

FIG. 4. Single rung on sublattice $\mathcal{A}$.

Neither of these exact eigenstates, however, is suited as a fiducial state for spin wave theory. We are hence led to define a vacuum state

$$|\tilde{b}_{-1/2}\rangle \equiv |b_{-1/2}\rangle \cos\phi + |c_{-1/2}\rangle \sin\phi$$
$$= \left(|\uparrow\downarrow\downarrow\rangle + |\downarrow\downarrow\uparrow\rangle\right)\left(-\tfrac{1}{\sqrt{6}}\cos\phi + \tfrac{1}{\sqrt{3}}\sin\phi\right)$$
$$+ |\downarrow\uparrow\downarrow\rangle\left(\sqrt{\tfrac{2}{3}}\cos\phi + \tfrac{1}{\sqrt{3}}\sin\phi\right), \quad (5)$$

which interpolates between the quantum ground state $|b_{-1/2}\rangle$ of the isolated rung with $S^z = -\frac{1}{2}$ for $\phi = 0$ and the classically Néel ordered state $\Downarrow\uparrow\downarrow\rangle$ for $\phi = \arctan(\frac{1}{\sqrt{2}}) = 0.6155$. The parameter ϕ will depend on the coupling between the rungs and the ladders. The motivation for introducing the state $|\tilde{b}_{-1/2}\rangle$ will become clear as we determine ϕ self-consistently below.

Since we wish $|\tilde{b}_{-1/2}\rangle$ to be one of our basis states, we replace (3) by

$$M^{\mathcal{A}} = \{|\mu\rangle^{\mathcal{A}}; \mu = 1,\ldots,8\}$$
$$= \{|\tilde{b}_{-1/2}\rangle, |b_{1/2}\rangle, |a_{-1/2}\rangle, |a_{1/2}\rangle,$$
$$|c_{-3/2}\rangle, |\tilde{c}_{-1/2}\rangle, |c_{1/2}\rangle, |c_{3/2}\rangle\}, \quad (6)$$

with

$$\begin{pmatrix} |b_{-1/2}\rangle \\ |c_{-1/2}\rangle \end{pmatrix} = \begin{pmatrix} u & -v \\ v & u \end{pmatrix}\begin{pmatrix} |\tilde{b}_{-1/2}\rangle \\ |\tilde{c}_{-1/2}\rangle \end{pmatrix} \quad (7)$$

and $u = \cos\phi$, $v = \sin\phi$. The relevant terms in the Hamiltonian (4) transform into

$$\left(|b_{-1/2}\rangle, |c_{-1/2}\rangle\right)\begin{pmatrix} -1 & 0 \\ 0 & \frac{1}{2} \end{pmatrix}\begin{pmatrix} \langle b_{-1/2}| \\ \langle c_{-1/2}| \end{pmatrix}$$
$$= \left(|\tilde{b}_{-1/2}\rangle, |\tilde{c}_{-1/2}\rangle\right)\begin{pmatrix} \frac{1}{2} - \frac{3}{2}u^2 & \frac{3}{2}uv \\ \frac{3}{2}uv & -1 + \frac{3}{2}u^2 \end{pmatrix}\begin{pmatrix} \langle \tilde{b}_{-1/2}| \\ \langle \tilde{c}_{-1/2}| \end{pmatrix}. \quad (8)$$

As a next step, we introduce bosonic creation and annihilation operators $a_0^\dagger \equiv |a_{-1/2}\rangle\langle\tilde{b}_{-1/2}|$, etc., as indicated in Fig. 5. The subscripts of these operators refer to the change in the z component of the total spin on the rung. Note that these operators do not obey the commutation relations of independent ladder operators, as we can create only one "particle" with either $a_0^\dagger$ or $a_1^\dagger$ or any other creation operator from the "vacuum" state $|\tilde{b}_{-1/2}\rangle$.

Completeness and orthonormality of the basis (6) implies

$$|\tilde{b}_{-1/2}\rangle\langle\tilde{b}_{-1/2}| = \left(1 - b_1^\dagger b_1 - a_0^\dagger a_0 - a_1^\dagger a_1 - c_{-1}^\dagger c_{-1} - c_0^\dagger c_0 - c_1^\dagger c_1 - c_2^\dagger c_2\right). \quad (9)$$

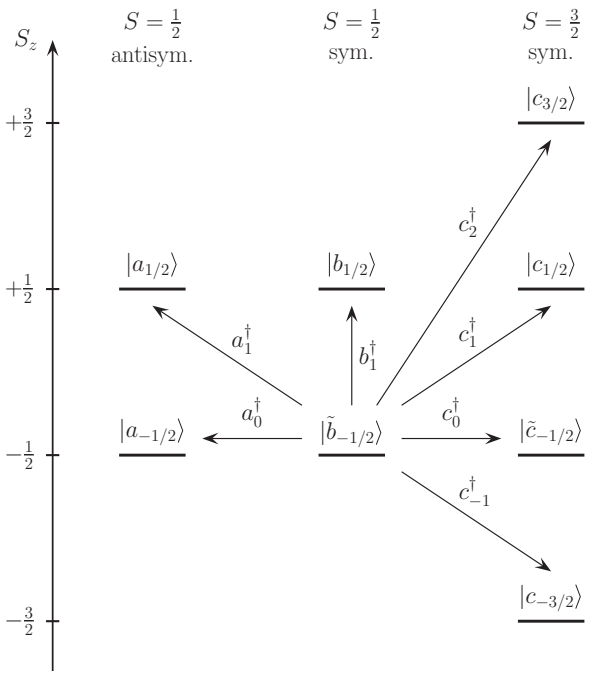

FIG. 5. Bosonic operator for sublattice $\mathcal{A}$.

With (7) and (9), the rung Hamiltonian (4) may be rewritten in terms of the bosonic operators:

$$\hat{H}^{\mathcal{A}} = \left(\frac{1}{2} - \frac{3}{2}u^2\right) + \left(-\frac{1}{2} + \frac{3}{2}u^2\right)\left(a_0^\dagger a_0 + a_1^\dagger a_1\right)$$
$$+ \tfrac{3}{2}uv\left(c_0^\dagger + c_0\right) + \tfrac{3}{2}\left(u^2 - v^2\right)c_0^\dagger c_0$$
$$- \tfrac{3}{2}v^2 b_1^\dagger b_1 + \tfrac{3}{2}u^2\left(c_{-1}^\dagger c_{-1} + c_1^\dagger c_1 + c_2^\dagger c_2\right). \quad (10)$$

On sublattice $\mathcal{B}$, we introduce a similar basis $M^{\mathcal{B}}$, with the only difference that the fiducial state $|\tilde{b}_{1/2}\rangle$ has $S^z = \frac{1}{2}$ instead of $s^z = -\frac{1}{2}$ for $|\tilde{b}_{-1/2}\rangle$ on sublattice $\mathcal{A}$:

$$M^{\mathcal{B}} = \{|\mu\rangle^{\mathcal{B}}; \mu = 1,\ldots,8\}$$
$$= \{|\tilde{b}_{1/2}\rangle, |b_{-1/2}\rangle, |a_{1/2}\rangle, |a_{-1/2}\rangle,$$
$$|c_{3/2}\rangle, |\tilde{c}_{1/2}\rangle, |c_{-1/2}\rangle, |c_{-3/2}\rangle\}, \quad (11)$$

with

$$\begin{pmatrix} |b_{1/2}\rangle \\ |c_{1/2}\rangle \end{pmatrix} = \begin{pmatrix} u & -v \\ v & u \end{pmatrix}\begin{pmatrix} |\tilde{b}_{1/2}\rangle \\ |\tilde{c}_{1/2}\rangle \end{pmatrix}. \quad (12)$$

We introduce a second set of bosonic creation and annihilation operators $A_0^\dagger \equiv |a_{1/2}\rangle\langle\tilde{b}_{1/2}|$ etc., as indicated in Fig. 6.

The Hamiltonian $H^{\mathcal{B}}$ for a single rung belonging to sublattice $\mathcal{B}$ is in analogy to (10) given by

$$\hat{H}^{\mathcal{B}} = \left(\frac{1}{2} - \frac{3}{2}u^2\right) + \left(-\frac{1}{2} + \frac{3}{2}u^2\right)\left(A_{-1}^\dagger A_{-1} + A_0^\dagger A_0\right)$$
$$+ \tfrac{3}{2}uv\left(C_0^\dagger + C_0\right) + \tfrac{3}{2}\left(u^2 - v^2\right)C_0^\dagger C_0 - \tfrac{3}{2}v^2 B_{-1}^\dagger B_{-1}$$
$$+ \tfrac{3}{2}u^2\left(C_{-2}^\dagger C_{-2} + C_{-1}^\dagger C_{-1} + C_1^\dagger C_1\right). \quad (13)$$

For later purposes, we write the spin operators $\hat{s}_\alpha^\pm = \hat{s}_\alpha^x \pm i\hat{s}_\alpha^y$ and $\hat{s}_\alpha^z$ for the individual sites $\alpha = 1,2,3$ on rungs

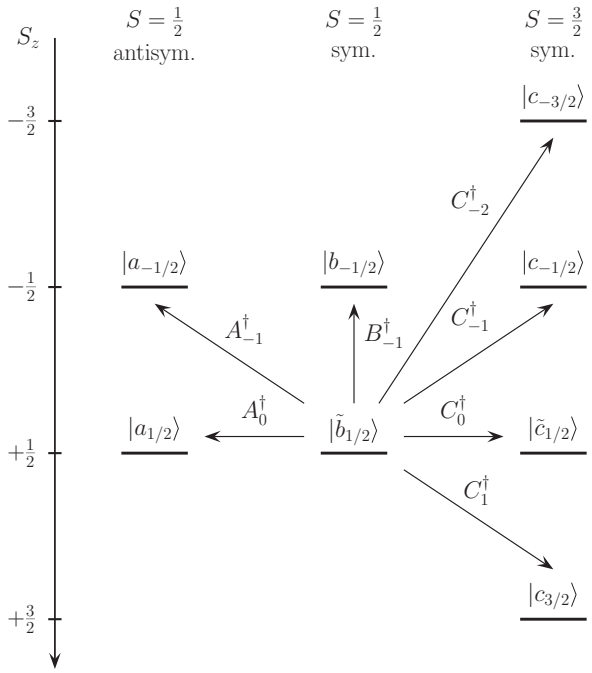

FIG. 6. Bosonic operator for sublattice $\mathcal{B}$.

belonging to sublattice $\mathcal{A}$ in terms of our bosonic creation and annihilation operators:

$$\begin{aligned}
\hat{s}^+_\alpha &= s^+_{\alpha,21}b^\dagger_1 + s^+_{\alpha,41}a^\dagger_1 + s^+_{\alpha,71}c^\dagger_1 + s^+_{\alpha,15}c_{-1} + s^+_{\alpha,82}c^\dagger_2 b_1 \\
&\quad + s^+_{\alpha,23}b^\dagger_1 a_0 + s^+_{\alpha,43}a^\dagger_1 a_0 + s^+_{\alpha,73}c^\dagger_1 a_0 + s^+_{\alpha,84}c^\dagger_2 a_1 \\
&\quad + s^+_{\alpha,35}a^\dagger_0 c_{-1} + s^+_{\alpha,65}c^\dagger_0 c_{-1} + s^+_{\alpha,26}b^\dagger_1 c_0 \\
&\quad + s^+_{\alpha,46}a^\dagger_1 c_0 + s^+_{\alpha,76}c^\dagger_1 c_0 + s^+_{\alpha,87}c^\dagger_2 c_1, \\
\hat{s}^-_\alpha &= \left(\hat{s}^+_\alpha\right)^\dagger, \qquad (14) \\
\hat{s}^z_\alpha &= s^z_{\alpha,11}\left(1 - b^\dagger_1 b_1 - a^\dagger_0 a_0 - a^\dagger_1 a_1\right. \\
&\quad \left. - c^\dagger_0 c_0 - c^\dagger_1 c_1 - c^\dagger_{-1} c_{-1} - c^\dagger_2 c_2\right) \\
&\quad + s^z_{\alpha,22}b^\dagger_1 b_1 + s^z_{\alpha,55}c^\dagger_{-1}c_{-1} + s^z_{\alpha,66}c^\dagger_0 c_0 \\
&\quad + s^z_{\alpha,77}c^\dagger_1 c_1 + s^z_{\alpha,88}c^\dagger_2 c_2 \\
&\quad + s^z_{\alpha,13}\left(a^\dagger_0 + a_0\right) + s^z_{\alpha,16}\left(c^\dagger_0 + c_0\right) \\
&\quad + s^z_{\alpha,27}\left(b^\dagger_1 c_1 + c^\dagger_1 b_1\right) + s^z_{\alpha,24}\left(b^\dagger_1 a_1 + a^\dagger_1 b_1\right) \\
&\quad + s^z_{\alpha,36}\left(a^\dagger_0 c_0 + c^\dagger_0 a_0\right) + s^z_{\alpha,47}\left(a^\dagger_1 c_1 + c^\dagger_1 a_1\right).
\end{aligned}$$

The matrix elements

$$s^\tau_{\alpha,\mu\nu} = \langle\mu|\hat{s}^\tau_\alpha\,|\nu\rangle^{\mathcal{A}} \quad \text{with} \quad \tau = +, -, z, \qquad (15)$$

and $|\mu\rangle^{\mathcal{A}}$ as defined in (6) are written out explicitly in Appendix A.

Similarly, the individual spin-operators $\hat{S}^\pm_\alpha$ on rungs belonging to sublattice $\mathcal{B}$ are given by

$$\begin{aligned}
\hat{S}^-_\alpha &= S^-_{\alpha,21}B^\dagger_{-1} + S^-_{\alpha,41}A^\dagger_{-1} + S^-_{\alpha,71}C^\dagger_{-1} + S^-_{\alpha,15}C_1 \\
&\quad + S^-_{\alpha,82}C^\dagger_{-2}B_{-1} + S^-_{\alpha,23}B^\dagger_{-1}A_0 + S^-_{\alpha,43}A^\dagger_{-1}A_0 \\
&\quad + S^-_{\alpha,73}C^\dagger_{-1}A_0 + S^-_{\alpha,84}C^\dagger_{-2}A_{-1} + S^-_{\alpha,35}A^\dagger_0 C_1 \\
&\quad + S^-_{\alpha,65}C^\dagger_0 C_1 + S^-_{\alpha,26}B^\dagger_{-1}C_0 + S^-_{\alpha,46}A^\dagger_{-1}C_0 \\
&\quad + S^-_{\alpha,76}C^\dagger_{-1}C_0 + S^-_{\alpha,87}C^\dagger_{-2}C_{-1}, \\
\hat{S}^+_\alpha &= \left(\hat{S}^-_\alpha\right)^\dagger, \qquad (16) \\
\hat{S}^z_\alpha &= S^z_{\alpha,11}\left(1 - B^\dagger_{-1}B_{-1} - A^\dagger_0 A_0 - A^\dagger_{-1}A_{-1}\right. \\
&\quad \left. - C^\dagger_0 C_0 - C^\dagger_{-1}C_{-1} - C^\dagger_1 C_1 - C^\dagger_{-2}C_{-2}\right) \\
&\quad + S^z_{\alpha,22}B^\dagger_{-1}B_{-1} + S^z_{\alpha,55}C^\dagger_1 C_1 + S^z_{\alpha,66}C^\dagger_0 C_0 \\
&\quad + S^z_{\alpha,77}C^\dagger_{-1}C_{-1} + S^z_{\alpha,88}C^\dagger_{-2}C_{-2} \\
&\quad + S^z_{\alpha,13}\left(A^\dagger_0 + A_0\right) + S^z_{\alpha,16}\left(C^\dagger_0 + C_0\right) \\
&\quad + S^z_{\alpha,27}\left(B^\dagger_{-1}C_{-1} + C^\dagger_{-1}B_{-1}\right) \\
&\quad + S^z_{\alpha,24}\left(B^\dagger_{-1}A_{-1} + A^\dagger_{-1}B_{-1}\right) \\
&\quad + S^z_{\alpha,36}\left(A^\dagger_0 C_0 + C^\dagger_0 A_0\right) \\
&\quad + S^z_{\alpha,47}\left(A^\dagger_{-1}C_{-1} + C^\dagger_{-1}A_{-1}\right),
\end{aligned}$$

with $S^\tau_{\alpha,\mu\nu} = \langle\mu|\hat{S}^\tau_\alpha\,|\nu\rangle^{\mathcal{B}}$ likewise given in Appendix A.

III. COUPLING THE RUNGS

As a microscopic model for site centered spin stripes, we couple the three-site rungs into three-leg ladders, with the spins coupled antiferromagnetically with J along the ladders and with J' between neighboring ladders, as shown in Fig. 7. The sublattice indices assigned to each rung alternate in both directions, i.e., under translation by either of the primitive lattice vectors $\hat{\boldsymbol{x}} = (4a, 0)$ or $\hat{\boldsymbol{y}} = (0, a)$, where a is the lattice constant we herewith set to unity. The microscopic model is hence given

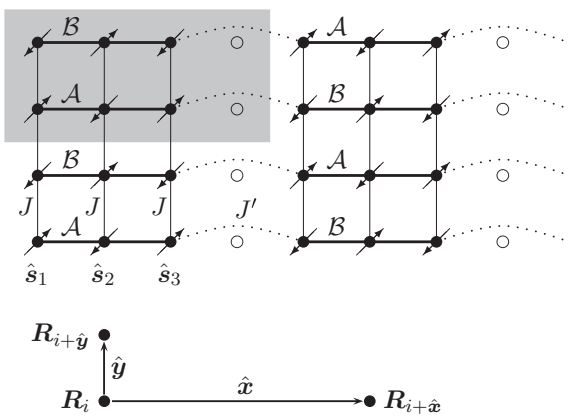

FIG. 7. The microscopic model for site centered spin stripes, with intrarung couplings set to unity, inter-rung–intraladder couplings J, and interladder couplings J'. The real space unit cell contains two rungs and is indicated by the shaded area in gray.

by the Hamiltonian

$$\hat{H} = \sum_{i\in\mathcal{A}} \left(\hat{H}_i^{\mathcal{A}} + J \sum_{\alpha=1}^{3} \hat{\mathbf{s}}_{\alpha i} \hat{\mathbf{S}}_{\alpha i+\hat{\mathbf{y}}} + J' \hat{\mathbf{s}}_{3i} \hat{\mathbf{S}}_{1 i+\hat{\mathbf{x}}} \right) + \sum_{j\in\mathcal{B}} \left(\hat{H}_j^{\mathcal{B}} + J \sum_{\alpha=1}^{3} \hat{\mathbf{S}}_{\alpha j} \hat{\mathbf{s}}_{\alpha j+\hat{\mathbf{y}}} + J' \hat{\mathbf{S}}_{3 j} \hat{\mathbf{s}}_{1 j+\hat{\mathbf{x}}} \right). \quad (17)$$

When evaluating the spectrum of (17) below, we will set $J = 1$ (and thereby equal to the intrarung couplings). The interladder coupling J' is determined numerically by comparing the energy difference of a t-J model with a charge stripe with and without frustrated boundary conditions to the corresponding difference in a Heisenberg model, in which the charge stripe has been replaced by an antiferromagnetic coupling J' (see Appendix B); we find $J' = 0.07$. For the moment, however, we keep the inter-rung and inter-ladder couplings J and J' as free parameter, as this makes it easier to trace the individual terms in the expansion below.

The next step is to expand (17) in terms of our bosonic creation and annihilation operators, using (14), (16), and

$$\boldsymbol{s}_\alpha \boldsymbol{S}_\beta = \frac{1}{2}\left(\hat{s}_\alpha^+ \hat{S}_\beta^- + \hat{s}_\alpha^- \hat{S}_\beta^+ \right) + \hat{s}_\alpha^z \hat{S}_\beta^z. \quad (18)$$

We keep only terms up to second order in the operators. Since $\hat{s}_\alpha^z$ (and $\hat{S}_\alpha^z$) contains a constant term with coefficient $s_{\alpha,11}^z$ as well as the linear terms

$$s_{\alpha,13}^z \left(a_0^\dagger + a_0 \right) + s_{\alpha,16}^z \left(c_0^\dagger + c_0 \right),$$

the expanded Hamiltonian will contain the linear term

$$\left[2J \sum_{\alpha=1}^{3} S_{\alpha,11}^z s_{\alpha,16}^z + J' \left(S_{1,11}^z s_{3,16}^z + S_{3,11}^z s_{1,16}^z \right] \right) \left(c_0^\dagger + c_0 \right) \quad (19)$$

in addition to the linear term

$$\frac{3}{2} u v \left(c_0^\dagger + c_0 \right) \quad (20)$$

already contained in (10) for each rung i on sublattice $\mathcal{A}$. The terms proportional to

$$\left(a_0^\dagger + a_0 \right)$$

cancel since $s_{1,13}^z = -s_{3,13}^z$ and $s_{2,13}^z = 0$. This cancellation can also be inferred from symmetry considerations, as elaborated in the following section.

We eliminate the linear terms (19) and (20) by adjusting the parameter ϕ, i.e., by solving

$$\frac{3}{2} u v + 2J \sum_{\alpha=1}^{3} S_{\alpha,11}^z s_{\alpha,16}^z + 2J' S_{1,11}^z s_{3,16}^z = 0 \quad (21)$$

with $J = 1$, $J' = 0.07$, $u = \cos\phi$, $v = \sin\phi$, and the matrix elements $s_{\alpha,\mu\nu}^z$ as given in Appendix A in terms of u and v. This yields

$$\sqrt{2}\frac{v}{u} \approx 0.5019 \quad \text{or} \quad \phi = 0.3410. \quad (22)$$

On a formal level, the reason for rotating our basis states via (5), (7), and (12) to begin with was that this created the linear term (20) in $H^{\mathcal{A}}$. Without this term, there would have been no way to eliminate (19), and the basis set would have been highly impractical for further analysis. On a physical level, the spontaneous breakdown of the SU(2) spin rotation symmetry leads us to expect that the fiducial state of the rungs is much closer to the classically ordered Néel state $|\uparrow\downarrow\uparrow\rangle$ than $|b_{-1/2}\rangle$. Not surprisingly, the spectrum evaluated below is gapless at some point in the Brillouin zone, as required by Goldstone's theorem for a state with a spontaneously broken continuous symmetry, if and only if ϕ assumes the value (22).

IV. EXPANDING THE HAMILTONIAN

To evaluate the spectrum of (17), we first define momentum space operators on sublattice $\mathcal{A}$ according to

$$a_{0,k} = \sqrt{\frac{2}{N}} \sum_{i\in\mathcal{A}} e^{ikR_i} a_{0,i},$$
$$a_{0,i} = \sqrt{\frac{2}{N}} \sum_{k} e^{-ikR_i} a_{0,k}, \quad (23)$$

where where N denotes the number of rungs and the sums over $\boldsymbol{k}$ are taken over the reduced Brillouin zone indicated in gray in Fig. 8. Similarly, for the creation and annihilation operators on sublattice $\mathcal{B}$ we introduce

$$A_{0,k} = \sqrt{\frac{2}{N}} \sum_{j\in\mathcal{B}} e^{-ikR_j} A_{0,j},$$
$$A_{0,j} = \sqrt{\frac{2}{N}} \sum_{k} e^{ikR_j} A_{0,k}, \quad (24)$$

which differ from (23) only in that the sign of the phases is reversed. Since we are only interested in the one-particle spin wave spectrum, we neglect the effect of the Hilbert space restrictions for the real space creation and annihilation operators (i.e., that we could create only one "particle" per rung) on the momentum space operators.

As mentioned above, we only keep terms up to second order in the creation and annihilation operators in the Hamiltonian. When substituting the explicit expressions (14) and (16) into

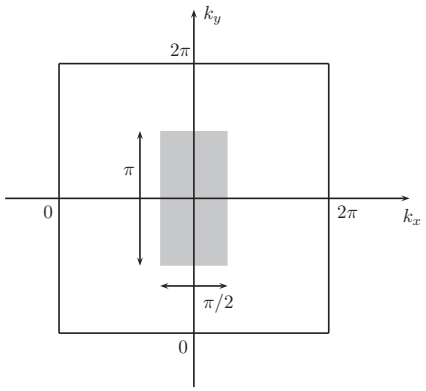

FIG. 8. The reduced Brillouin zone corresponding to the real space unit cell indicated in Fig. 7 contains only one-eighth of the full Brillouin zone and is indicated by the shaded area.

(17), we see immediately that many terms yield only higher orders, while others cancel. To begin with, since the spin flip operators only contain terms of first and second order in the creation and annihilation operators and are always multiplied with another spin-flip operator, we only need to keep terms of first order in the expressions for $\hat{s}^+_\alpha$ and $\hat{S}^-_\alpha$. The expansions of the $\hat{s}^z_\alpha \hat{S}^z_\beta$ terms are slightly more complicated, as $\hat{s}^z_\alpha$ and $\hat{S}^z_\beta$ contain constant terms in addition to terms of first and second order in the creation and annihilation operators. We have adjusted the parameter ϕ such that the linear terms in the expansion cancel. Most of the quadratic terms result from multiplying the constant term $S^z_{\alpha,11}$ in the expansion of $\hat{S}^z_\alpha$ with the quadratic terms in $\hat{s}^z_\alpha$ and multiplying $s^z_{\alpha,11}$ with quadratic terms in $\hat{S}^z_\alpha$. This yields seven diagonal terms (like $b^\dagger_1 b_1$) and four off-diagonal terms (like $b^\dagger_1 c_1 + c^\dagger_1 b_1$) for each sublattice. Three of the off-diagonal terms, those linear in the antisymmetric operators $a^\dagger_1$ or a_1, vanish. This can be seen either from the explicit coefficients written out in Appendix A (e.g., $s^z_{1,24} = -s^z_{3,24}$ and $s^z_{2,24} = 0$ while $S^z_{1,11} = S^z_{3,11}$) or from a symmetry consideration. As the Hamiltonian is invariant under reflection symmetry interchanging the outer chains of each three-leg ladder (i.e., sites 1 and 3 on each rung), there can only be terms containing an even number of the antisymmetric operators $a^\dagger_0, a_0, a^\dagger_1, a_1, A^\dagger_0, A_0, A^\dagger_{-1}$, or A_{-1} in the expansion.

In addition to this reflection symmetry, we have the SU(2) spin rotation symmetry of the Hamiltonian (17). The spin symmetry implies that the z component of the total spin,

$$\hat{S}^z_{\text{tot}} = \sum_{i\in\mathcal{A}} \hat{s}^z_{\alpha i} + \sum_{j\in\mathcal{B}} \hat{S}^z_{\alpha j}, \tag{25}$$

must be conserved. This means that to second order in the creation and annihilation operators, only operators which change $\hat{s}^z$ or $\hat{S}^z$ by the same integer can appear in each term. For example, we can have a term $b^\dagger_1 c_1$ or $b^\dagger_1 c^\dagger_{-1}$, but not $b^\dagger_1 c_0$. Both symmetries together imply that to second order, the Hamiltonian (17) decomposes into terms which contain only operators belonging to one particular group,

$$\hat{H} = \tilde{E}_0 + \hat{H}_{a0} + \hat{H}_{c0} + \hat{H}_{a1} + \hat{H}_{c2} + \hat{H}_{b1,c1,c-1}, \tag{26}$$

where $\tilde{E}_0$ is a contribution to the ground state energy, $\hat{H}_{a0}$ contains only the operators $a^\dagger_0$, a_0, $A^\dagger_0$, and A_0, and so on. The low energy physics we are interested in is contained in $\hat{H}_{b1,c1,c-1}$, which we will analyze in detail below. As for the other terms, explicit expressions and expansions in terms of creation and annihilation operators are given in Appendix C. $\hat{H}_{a0}$ and $\hat{H}_{c0}$ describe almost dispersionless modes with energies of around 2.1 and 2.7 (in units of J_{exp} which we eventually set to $J_{\text{exp}} = 140\,\text{meV}$). $\hat{H}_{a1}$ describes a weakly dispersing mode of energy of about 2.0, with a bandwidth of about 0.2. $\hat{H}_{c_2}$ describes a completely dispersionless mode with energy 3.12. Cuts of the dispersions of these modes are shown in Fig. 16 in Appendix C. Since these modes occur at energies at which we consider our spin wave theory no longer reliable, we will not discuss them further.

To evaluate the spectrum of $\hat{H}_{b1,c1,c-1}$, we write

$$\hat{H}_{b1,c1,c-1} = \sum_k \left(\hat{\Psi}^\dagger_k H_k \hat{\Psi}_k - \frac{1}{2}\text{tr}(H_k) \right), \tag{27}$$

where

$$\hat{\Psi}^\dagger_k = \left(B^\dagger_{-1,k}, b_{1,k}, C^\dagger_{-1,k}, c_{1,k}, C_{1,-k}, c^\dagger_{-1,-k} \right),$$

$$\hat{\Psi}_k = \left(B_{-1,k}, b^\dagger_{1,k}, C_{-1,k}, c^\dagger_{1,k}, C^\dagger_{1,-k}, c_{-1,-k} \right)^{\text{T}}. \tag{28}$$

The 6×6 matrix H_k consists of the k-independent diagonal terms

$$\begin{aligned}
H_{k,11} = H_{k,22} &= -\frac{3}{2}v^2 + 2J \sum_{\alpha=1}^{3} s^z_{\alpha,11}(S^z_{\alpha,22} - S^z_{\alpha,11}) \\
&\quad + 2J' s^z_{3,11}(S^z_{1,22} - S^z_{1,11}), \\
H_{k,33} = H_{k,44} &= \frac{3}{2}u^2 + 2J \sum_{\alpha=1}^{3} s^z_{\alpha,11}(S^z_{\alpha,77} - S^z_{\alpha,11}) \\
&\quad + 2J' s^z_{3,11}(S^z_{1,77} - S^z_{1,11}), \\
H_{k,55} = H_{k,66} &= \frac{3}{2}u^2 + 2J \sum_{\alpha=1}^{3} s^z_{\alpha,11}(S^z_{\alpha,55} - S^z_{\alpha,11}) \\
&\quad + 2J' s^z_{3,11}(S^z_{1,55} - S^z_{1,11}).
\end{aligned} \tag{29}$$

The off-diagonal terms are of the general form

$$H_{k,ij} = H_{k,ji} = H^0_{ij} + H^x_{ij} \cos(4k_x) + H^y_{ij} \cos(k_y).$$

The k-independent coefficients

$$H^0_{13} = H^0_{24} = 2J \sum_{\alpha=1}^{3} s^z_{\alpha,11} S^z_{\alpha,27} + 2J' s^z_{3,11} S^z_{1,27} \tag{30}$$

result from the $\hat{s}^z_\alpha \hat{S}^z_\beta$ terms. Expansion of the $\hat{s}^+_\alpha \hat{S}^-_\beta$ terms yields the coefficients

$$\begin{aligned}
H^x_{12} &= J' s^+_{3,21} S^-_{1,21}, & H^x_{14} &= J' s^+_{3,71} S^-_{1,21}, \\
H^x_{16} &= J' s^+_{3,15} S^-_{1,21}, & H^x_{23} &= J' s^-_{3,21} S^+_{1,71}, \\
H^x_{25} &= J' s^-_{3,21} S^+_{1,51}, & H^x_{34} &= J' s^+_{3,71} S^-_{1,71}, \\
H^x_{36} &= J' s^+_{3,15} S^-_{1,71}, & H^x_{45} &= J' s^-_{3,71} S^+_{1,51}, \\
H^x_{56} &= J' s^+_{3,15} S^-_{1,15}, &&
\end{aligned} \tag{31}$$

and

$$\begin{aligned}
H^y_{12} &= J \sum_{\alpha=1}^{3} s^+_{\alpha,21} S^-_{\alpha,21}, & H^y_{14} &= J \sum_{\alpha=1}^{3} s^+_{\alpha,71} S^-_{\alpha,21}, \\
H^y_{16} &= J \sum_{\alpha=1}^{3} s^+_{\alpha,15} S^-_{\alpha,21}, & H^y_{23} &= J \sum_{\alpha=1}^{3} s^-_{\alpha,12} S^+_{\alpha,17}, \\
H^y_{25} &= J \sum_{\alpha=1}^{3} s^+_{\alpha,21} S^-_{\alpha,15}, & H^y_{34} &= J \sum_{\alpha=1}^{3} s^+_{\alpha,71} S^-_{\alpha,71}, \\
H^y_{36} &= J \sum_{\alpha=1}^{3} s^+_{\alpha,15} S^-_{\alpha,71}, & H^y_{45} &= J \sum_{\alpha=1}^{3} s^-_{\alpha,17} S^+_{\alpha,51}, \\
H^y_{56} &= J \sum_{\alpha=1}^{3} s^+_{\alpha,15} S^-_{\alpha,15}. &&
\end{aligned} \tag{32}$$

All other off-diagonal elements of $H_{k,ij}$ vanish.

V. SOLUTION BY BOGOLIUBOV TRANSFORMATION

The Hamiltonian (27) can be diagonalized with a $2n$–dimensional Bogoliubov transformation.[38] We begin with a brief review of the formalism.

At each point in k space, we wish to write the Hamiltonian in terms of a diagonal matrix Ω,

$$\hat{H} = \hat{\Psi}^\dagger H \hat{\Psi} = \hat{\Gamma}^\dagger \Omega \hat{\Gamma}, \tag{33}$$

with

$$\hat{\Psi} = M\hat{\Gamma}, \qquad \Omega = M^\dagger H M. \tag{34}$$

The components of $\hat{\Gamma}$ satisfy the same commutation relations as the components of $\hat{\Psi}$:

$$\left[\hat{\Psi}_i, \hat{\Psi}_j^\dagger\right] = \left[\hat{\Gamma}_i, \hat{\Gamma}_j^\dagger\right] = T_{ij} \tag{35}$$

with

$$T = \mathrm{diag}\,(1, -1, 1, -1, -1, 1)\,. \tag{36}$$

This implies

$$T_{ij} = \left[\hat{\Psi}_i, \hat{\Psi}_j^\dagger\right] = \sum_{l,m} \left[M_{il}\hat{\Gamma}_l, \hat{\Gamma}_m^\dagger (M^\dagger)_{mj}\right]$$
$$= \sum_{l,m} M_{il}\left[\hat{\Gamma}_l, \hat{\Gamma}_m^\dagger\right] M_{mj}^\dagger = \sum_{l,m} M_{il} T_{lm} M_{mj}^\dagger,$$

or

$$T = MTM^\dagger. \tag{37}$$

Multiplying (37) by HM yields, with (34),

$$THM = MT\Omega, \tag{38}$$

or in components

$$\sum_l (TH)_{il} M_{lj} = M_{ij} (T\Omega)_{jj}, \tag{39}$$

i.e., the jth column of M is given by an eigenvector of TH with eigenvalue $T_{jj}\Omega_{jj}$. This specifies M up to the normalization of the eigenvectors. To obtain the normalization, it is propitious to rewrite (37) as

$$T = M^\dagger T M. \tag{40}$$

[To obtain (40), multiply (37) by TM^{-1} from the left and by TM from the right and use $T^2 = 1$.] Each column j of M_{ij} must hence be normalized such that

$$T_{jj} = \sum_i T_{ii} |M_{ij}|^2. \tag{41}$$

Diagonalization of (27) using this formalism at each point in k space with

$$\hat{\Gamma}_k^\dagger = \left(\gamma_{1,k}^\dagger, \gamma_{2,k}, \gamma_{3,k}^\dagger, \gamma_{4,k}, \gamma_{5,k}, \gamma_{6,k}^\dagger\right),$$
$$\hat{\Gamma}_k = \left(\gamma_{1,k}, \gamma_{2,k}^\dagger, \gamma_{3,k}, \gamma_{4,k}^\dagger, \gamma_{5,k}^\dagger, \gamma_{6,k}\right)^{\mathrm{T}} \tag{42}$$

yields

$$\hat{H}_{b1,c1,c-1} = \sum_{k,i} \left[\omega_{k,i}\, \gamma_{i,k}^\dagger \gamma_{i,k} + \frac{1}{2}\left(\omega_{k,i} - H_{k,ii}\right)\right]. \tag{43}$$

This Hamiltonian describes three twofold degenerate modes $\omega_{\boldsymbol{k},i}$, which we have plotted assuming $J_{\mathrm{exp.}} = 140$ meV as cuts along (k_x, π) and (π, k_y) in Fig. 9. The twofold degeneracy of each mode corresponds to spin waves with $S_z = \pm 1$. Since we expect our spin wave theory to be reliable only for energies up to $J_{\mathrm{exp.}}$, we will disregard the higher modes along with those

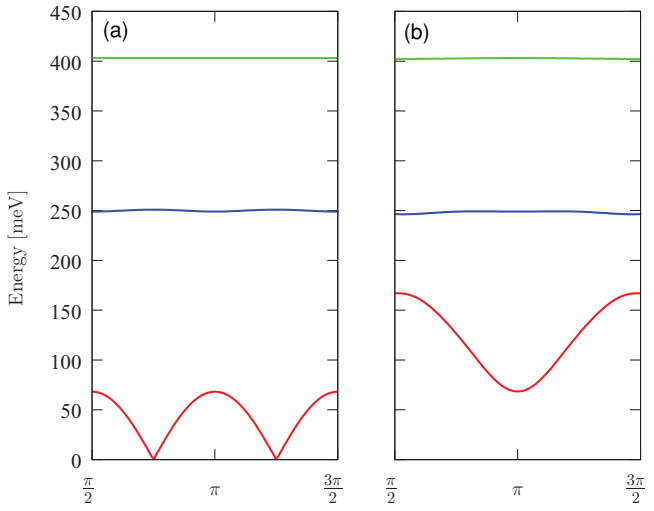

FIG. 9. (Color online) Modes described by $\hat{H}_{b1,c1,c-1}$ plotted as cuts (a) along (k_x, π) and (b) along (π, k_y) using $J_{\mathrm{exp}} = 140$ meV.

analyzed in Appendix C. The lowest mode $\omega_{\boldsymbol{k},1} = \omega_{\boldsymbol{k},2} := \omega(\boldsymbol{k})$ is shown as a 3D plot for half of the reduced Brillouin zone in Fig. 10.

The Hamiltonian (43) further contains a contribution

$$E_{b1,c1,c-1} = \sum_{k,i} \frac{1}{2}\left(\omega_{k,i} - H_{k,ii}\right) = -0.22116\, N \tag{44}$$

to the ground-state energy. (Here N denotes the number of rungs. The sum extends over $\frac{N}{2}$ values for $\boldsymbol{k}$.) In Appendix D, we obtain the ground-state energy by adding this contribution to the contributions of the other terms in (26) given in Appendix C, and obtain $E_0 = -1.73378\, N$. We find that this number is in excellent agreement with what we would expect from diagonalizing the model for a finite cluster with unfrustrated boundary conditions. This confirms the validity of our analysis.

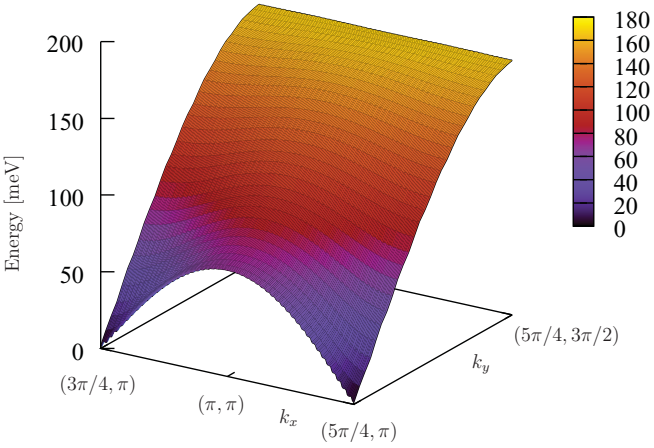

FIG. 10. (Color online) The dispersion $\omega(k_x, k_y)$ of the lowest eigenmode of $\hat{H}_{b1,c1,c-1}$ in half of the reduced Brillouin assuming $J_{\mathrm{exp.}} = 140$ meV.

VI. DISCUSSION OF THE RESULTS

A. Agreement with the experimental data

The significance of our results emerges in the context of a comparison of our spectrum with the experimental data obtained by Tranquada *et al.*[15] through inelastic neutron scattering on the stripe ordered compound $La_{1.875}Ba_{0.125}CuO_4$. The data points with their corresponding error bars are shown as black or blue crosses in Figs. 1(a) and 1(b), respectively.

In Fig. 1(b), which is directly reproduced from Tranquada *et al.*,[15] the neutron data are superposed with the spectrum of the triplet excitation of an isotropic two-leg Heisenberg ladder, which models bond centered stripes at accordingly high energies. In Fig. 1(a), we have superposed cuts of the lowest mode $\omega(\boldsymbol{k})$ along (k_x, π) and (π, k_y) with the experimental data. (The superposition of cuts of our spectrum in the x and y direction reflects the assumption that a superposition of domains with stripes along the two principal lattice directions has been observed in the experiment.) We believe it is fair to say that up to energies of about 180 meV, the agreement is excellent. (Above these energies, or more precisely above energies of order J, a perturbative spin wave analysis becomes unreliable.) Likewise, the constant energy slices of the neutron scattering intensities $\chi^{+-}(\boldsymbol{k},\omega)$ obtained with the matrix elements calculated in Appendix E shown in Fig. 11 agree very well with the experimentally measured constant-energy slices of the magnetic scattering in $La_{1.875}Ba_{0.125}CuO_4$ shown in Fig. 2 of Tranquada *et al.*[15]

B. Dependence on the interladder coupling J'

The good agreement of our results with the experimental data up to energies even larger than $J = 140$ meV (where we would expect that the perturbative spin-wave analysis becomes unreliable) is somewhat surprising. While any explanation in terms of bond-centered stripes through coupled two-leg ladders[15,23,24] gives immediately a roughly adequate estimate for the saddle-point energy in terms of the triplet energy gap of the individual two-leg ladders, it is far from obvious that a model of coupled three-leg ladders, which are individually gapless, should give a saddle-point energy consistent with the data. In our model, the saddle-point energy depends significantly on the coupling J' between the ladders. Fortunately, however, it is possible to determine J' rather accurately through numerical comparison of a t–J model with a site centered spin and a site centered charge stripe to a model with three-leg Heisenberg ladders coupled by J', as described in Appendix B. This analysis does not only provide us with the value $J' \approx 0.07J$, but also shows that this value is rather robust in the sense that it does not significantly depend on the details of how we localize the stripe. To obtain a better understanding of the dependence of our final results on this coupling, we have obtained the spectrum for a number of different values of J' by solving (21) numerically for each value, and proceeding with the Bogoliubov transformation with the resulting values for $u(J')$ and $v(J')$. The results for the saddle-point energies $\omega(\pi,\pi)$ are shown in Fig. 12 (black dots). Fitting the data yields

$$\omega(\pi,\pi) \approx 1.47\sqrt{J'J} \tag{45}$$

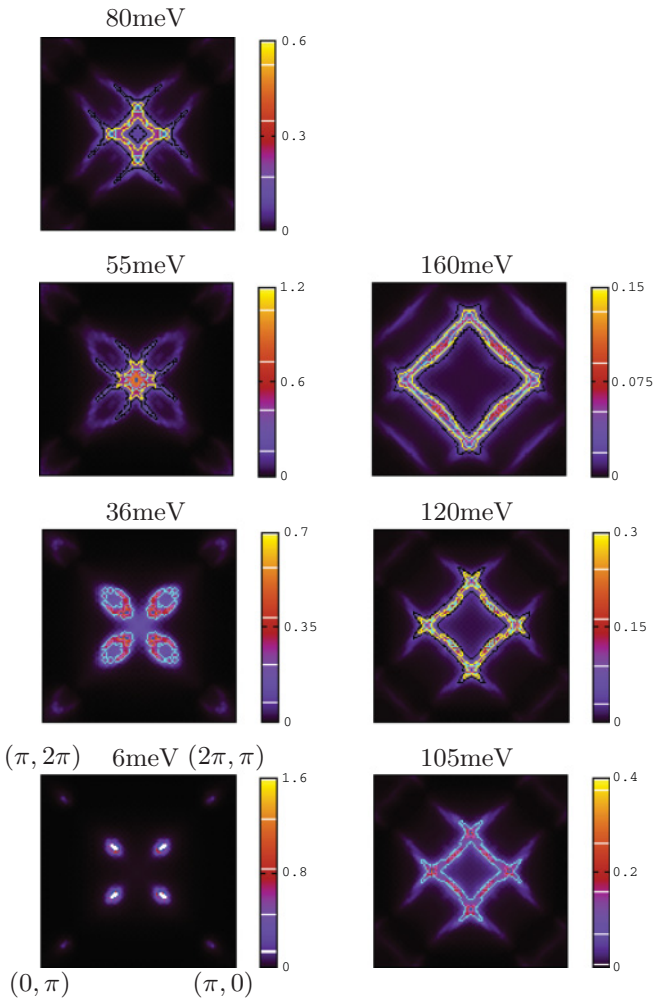

FIG. 11. (Color online) Constant energy slices of the neutron scattering intensity $\chi^{+-}(k,\omega)$ (see Appendix E below) for $J_{\text{exp}} = 140$ meV and $J' = 0.07\,J_{\text{exp}}$ in the magnetic Brillouin zone. In the indicated energy range, only the lowest mode shown in Figs. 10 and 1(a) contributes. We have replaced the δ-functions in frequency by Lorentzians with half-width $\Delta = 0.05\,J_{\text{exp}}$ and averaged over both stripe orientations (i.e., horizontal and vertical).

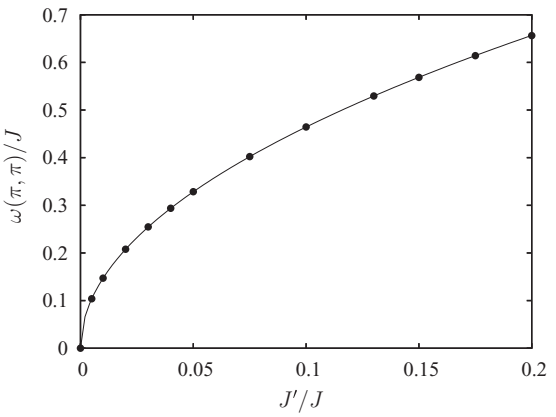

FIG. 12. (Color online) The saddle point energy $\omega(\pi,\pi)$ of the lowest magnetic mode $\omega(\boldsymbol{k})$ calculated for various values of J'/J (points). Fitting yields $\omega(\pi,\pi) \approx 1.47\sqrt{J'J}$ (solid line).

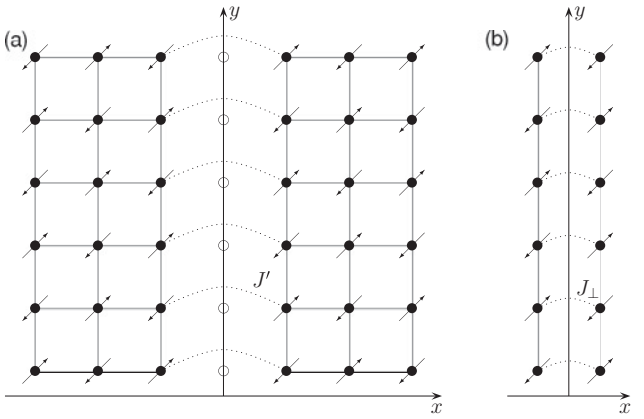

FIG. 13. Auxiliary models of (a) two weakly coupled three-leg ladders and (b) two weakly coupled spin $\frac{1}{2}$ chains used in the discussion to understand the square root dependence of $\omega(\pi,\pi)$ on J' depicted in Fig. 12.

to an excellent approximation up to values where J' becomes comparable to J (solid line).

The square-root dependence of $\omega(\pi,\pi)$ on J' can be understood by considering a model of two three-leg ladders, which are weakly coupled by J', as shown in Fig. 13(a). The low-energy excitations of the individual three-leg ladders are spin $\frac{1}{2}$ spinons, which are gapless. The coupling J' induces a linear confinement potential

$$V(y) = F|y| \tag{46}$$

between pairs of spinons, since the links coupling the chains effectively become decorrelated in the region between them. The situation here is similar to a system of two coupled spin $\frac{1}{2}$ chains shown in Fig. 13(b), where a weak coupling $J_\perp$ between the chains is known to induce a linear confinement potential between pairs of spinons.[18] In the model of coupled chains, the force between the spinons is proportional to[19,39]

$$F \approx \langle \boldsymbol{S}\boldsymbol{S}\rangle_\perp J_\perp \propto J_\perp^2/J. \tag{47}$$

For the model of two coupled three-leg ladders we consider here in the context of understanding the dependence (45) of our spin wave analysis, however, we assume that the spin correlation $\langle \boldsymbol{S}\boldsymbol{S}\rangle$ between the sites coupled by J' is to lowest order independent of J'/J. Therewith we account for the static correlations present due to the long range order we assume. For the confinement force in our auxiliary model of two coupled three-leg ladders we hence assume

$$F \propto J'. \tag{48}$$

The spinon confinement will then induce a gap Δ, which corresponds to the the ground state or zero-point energy of the linear potential oscillator for the relative motion of the spinons. The dispersion of the spinons is linear for both the individual spin chains and the individual three-leg ladders,[40]

$$\varepsilon(k_y) \approx v|k_y|, \tag{49}$$

with $v \propto J$ as J is the only energy scale is these models. [(In (49), we have shifted both spinon branches to the origin.] The ground-state energy E_0 of a constant force F oscillator of linearly dispersing particles with velocity v, however, is proportional to $\sqrt{Fv}$.[41] This implies $\Delta \propto J_\perp$ for the two weakly coupled chains and $\Delta \propto \sqrt{J'J}$ for the two weakly coupled three-leg ladders with the additional assumption of static correlations due to long range order.

To see why this gap Δ corresponds to the saddle point energy $\omega(\pi,\pi)$ in the spin-wave analysis above, consider the transformation properties of our auxiliary model of the two weakly coupled three-leg ladders shown in Fig. 13(a) under the parity reflection $x \to -x$. The gapped spinon-spinon bound state is odd under this symmetry, which in the language of momenta k_x of the site centered stripe model corresponds to a shift of $\frac{\pi}{4}$. Since the ground state of the stripe model has order with $k_x = \pi \pm \frac{\pi}{4}$, the gapped excitation will correspond to $k_x = \pi$. Following this line of reasoning, we can understand the square-root dependence (45) of $\omega(\pi,\pi)$ depicted in Fig. 12.

VII. CONCLUSIONS

In this work, we have provided a full and detailed account of a spin-wave analysis of a coupled three-leg ladder model for spin stripes in copper oxide superconductors. We have numerically evaluated the interladder coupling J' induced by the charge stripes in between both site-centered spin stripes modelled by three-leg ladders and bond-centered spin stripes modelled by two-leg ladders. As reported previously,[36] for the latter we obtain a ferromagnetic coupling $J' = -0.05J$, which is not sufficient to close the energy gap of the individual two-leg ladders. This does not imply that the stripes cannot be bond-centered. It does imply, however, that a description in terms of spin-only models of coupled two-leg ladders is not sensible.

For site-centered spin stripes modelled by three-leg ladders, we obtain an antiferromagnetic coupling $J' = 0.07J$. We have calculated the spectrum, the staggered magnetization, the dynamical structure factor $\chi^{+-}(\boldsymbol{k},\omega)$, and the ground-state energy for a spin-only model of coupled three-leg ladders using a linear spin wave analysis of bosonic operators representing the eight-dimensional Hilbert spaces on each three-site rung. The analysis makes no assumptions except for the model itself, and contains no variational parameter, as even the interladder coupling J' is evaluated through exact diagonalizations of small t–J clusters with and without charge stripes in between the spin stripes. We find excellent agreement with the experimental data of Tranquada *et al.*[15] The experimental data hence point toward site-centered, and not, as previously asserted, bond-centered[15,23,24] stripes.

ACKNOWLEDGMENTS

We wish to thank Matthias Vojta, Tobias Ulbricht, and Peter Wölfle for discussions of this work. This work was supported by the German Research Foundation under grant FOR 960.

APPENDIX A: MATRIX ELEMENTS OF THE INDIVIDUAL SPIN OPERATORS ON RUNGS

In Sec. II, we have written out the spin operators $\hat{s}^{\tau}_{\alpha}$ and $\hat{S}^{\tau}_{\alpha}$ with $\tau = +, -, z$ on the individual sites $\alpha = 1,2,3$ on rungs belonging to sublattice $\mathcal{A}$ and $\mathcal{B}$, respectively,

$$\hat{s}^{\tau}_{\alpha} = \sum_{\mu,\nu} s^{\tau}_{\alpha,\mu\nu} \, |\mu\rangle \, \langle\nu|^{\mathcal{A}}, \tag{A1}$$

$$\hat{S}^{\tau}_{\alpha} = \sum_{\mu,\nu} S^{\tau}_{\alpha,\mu\nu} \, |\mu\rangle \, \langle\nu|^{\mathcal{B}}, \tag{A2}$$

in the basis sets $M^{\mathcal{A}}$ and $M^{\mathcal{B}}$ specified in (6) and (11). The matrix elements,

$$s^{\tau}_{\alpha,\mu\nu} = \langle\mu|\hat{s}^{\tau}_{\alpha}\,|\nu\rangle^{\mathcal{A}}, \tag{A3}$$

$$S^{\tau}_{\alpha,\mu\nu} = \langle\mu|\hat{S}^{\tau}_{\alpha}\,|\nu\rangle^{\mathcal{B}}, \tag{A4}$$

are explicitly given by

$$s_1^+ = \begin{pmatrix} 0 & 0 & 0 & 0 & \frac{-u+\sqrt{2}v}{\sqrt{6}} & 0 & 0 & 0 \\ \frac{-2\sqrt{2}u+v}{3\sqrt{2}} & 0 & -\frac{1}{\sqrt{3}} & 0 & 0 & \frac{u+\sqrt{2}v}{3\sqrt{2}} & 0 & 0 \\ 0 & 0 & 0 & 0 & \frac{1}{\sqrt{2}} & 0 & 0 & 0 \\ -\frac{\sqrt{2}u+v}{\sqrt{6}} & 0 & 0 & 0 & 0 & \frac{-u+\sqrt{2}v}{\sqrt{6}} & 0 & 0 \\ 0 & 0 & 0 & 0 & 0 & 0 & 0 & 0 \\ 0 & 0 & 0 & 0 & \frac{\sqrt{2}u+v}{\sqrt{6}} & 0 & 0 & 0 \\ \frac{u+2\sqrt{2}v}{3\sqrt{2}} & 0 & -\frac{1}{\sqrt{6}} & 0 & 0 & \frac{2\sqrt{2}u-v}{3\sqrt{2}} & 0 & 0 \\ 0 & -\frac{1}{\sqrt{6}} & 0 & \frac{1}{\sqrt{2}} & 0 & 0 & \frac{1}{\sqrt{3}} & 0 \end{pmatrix} = \left(s_1^-\right)^{\dagger} = S_1^- = \left(S_1^+\right)^{\dagger}, \tag{A5}$$

$$s_2^+ = \begin{pmatrix} 0 & 0 & 0 & 0 & \frac{\sqrt{2}u+v}{\sqrt{3}} & 0 & 0 & 0 \\ \frac{u-\sqrt{2}v}{3} & 0 & 0 & 0 & 0 & -\frac{\sqrt{2}u+v}{3} & 0 & 0 \\ 0 & 0 & 0 & 0 & 0 & 0 & 0 & 0 \\ 0 & 0 & -1 & 0 & 0 & 0 & 0 & 0 \\ 0 & 0 & 0 & 0 & 0 & 0 & 0 & 0 \\ 0 & 0 & 0 & 0 & \frac{u-\sqrt{2}v}{\sqrt{3}} & 0 & 0 & 0 \\ \frac{-\sqrt{2}u+2v}{3} & 0 & 0 & 0 & 0 & \frac{2u+\sqrt{2}v}{3} & 0 & 0 \\ 0 & \sqrt{\frac{2}{3}} & 0 & 0 & 0 & 0 & \frac{1}{\sqrt{3}} & 0 \end{pmatrix} = \left(s_2^-\right)^{\dagger} = S_2^- = \left(S_2^+\right)^{\dagger}, \tag{A6}$$

$$s_3^+ = \begin{pmatrix} 0 & 0 & 0 & 0 & \frac{-u+\sqrt{2}v}{\sqrt{6}} & 0 & 0 & 0 \\ \frac{-2\sqrt{2}u+v}{3\sqrt{2}} & 0 & \frac{1}{\sqrt{3}} & 0 & 0 & \frac{u+\sqrt{2}v}{3\sqrt{2}} & 0 & 0 \\ 0 & 0 & 0 & 0 & -\frac{1}{\sqrt{2}} & 0 & 0 & 0 \\ \frac{\sqrt{2}u+v}{\sqrt{6}} & 0 & 0 & 0 & 0 & \frac{u-\sqrt{2}v}{\sqrt{6}} & 0 & 0 \\ 0 & 0 & 0 & 0 & 0 & 0 & 0 & 0 \\ 0 & 0 & 0 & 0 & \frac{\sqrt{2}u+v}{\sqrt{6}} & 0 & 0 & 0 \\ \frac{u+2\sqrt{2}v}{3\sqrt{2}} & 0 & \frac{1}{\sqrt{6}} & 0 & 0 & \frac{2\sqrt{2}u-v}{3\sqrt{2}} & 0 & 0 \\ 0 & -\frac{1}{\sqrt{6}} & 0 & -\frac{1}{\sqrt{2}} & 0 & 0 & \frac{1}{\sqrt{3}} & 0 \end{pmatrix} = \left(s_3^-\right)^{\dagger} = S_3^- = \left(S_3^+\right)^{\dagger}, \tag{A7}$$

$$s_1^z = \begin{pmatrix} -\frac{\left(\sqrt{2}u+v\right)^2}{6} & 0 & \frac{-u+\sqrt{2}v}{2\sqrt{3}} & 0 & 0 & \frac{-\sqrt{2}u^2+uv+\sqrt{2}v^2}{6} & 0 & 0 \\ 0 & \frac{1}{3} & 0 & \frac{1}{2\sqrt{3}} & 0 & 0 & \frac{1}{3\sqrt{2}} & 0 \\ \frac{-u+\sqrt{2}v}{2\sqrt{3}} & 0 & 0 & 0 & 0 & \frac{\sqrt{2}u+v}{2\sqrt{3}} & 0 & 0 \\ 0 & \frac{1}{3\sqrt{2}} & 0 & 0 & 0 & 0 & -\frac{1}{\sqrt{6}} & 0 \\ 0 & 0 & 0 & 0 & -\frac{1}{2} & 0 & 0 & 0 \\ \frac{-\sqrt{2}u^2+uv+\sqrt{2}v^2}{6} & 0 & \frac{\sqrt{2}u+v}{2\sqrt{3}} & 0 & 0 & -\frac{\left(u-\sqrt{2}v\right)^2}{6} & 0 & 0 \\ 0 & \frac{1}{3\sqrt{2}} & 0 & -\frac{1}{\sqrt{6}} & 0 & 0 & \frac{1}{6} & 0 \\ 0 & 0 & 0 & 0 & 0 & 0 & 0 & \frac{1}{2} \end{pmatrix} = -S_1^z, \tag{A8}$$

$$s_2^z = \begin{pmatrix} \frac{u^2+4\sqrt{2}uv-v^2}{6} & 0 & 0 & 0 & 0 & \frac{\sqrt{2}u^2-uv-\sqrt{2}v^2}{3} & 0 & 0 \\ 0 & -\frac{1}{6} & 0 & 0 & 0 & 0 & -\frac{\sqrt{2}}{3} & 0 \\ 0 & 0 & -\frac{1}{2} & 0 & 0 & 0 & 0 & 0 \\ 0 & 0 & 0 & \frac{1}{2} & 0 & 0 & 0 & 0 \\ 0 & 0 & 0 & 0 & -\frac{1}{2} & 0 & 0 & 0 \\ \frac{\sqrt{2}u^2-uv-\sqrt{2}v^2}{3} & 0 & 0 & 0 & 0 & \frac{-u^2-4\sqrt{2}uv+v^2}{6} & 0 & 0 \\ 0 & -\frac{\sqrt{2}}{3} & 0 & 0 & 0 & 0 & \frac{1}{6} & 0 \\ 0 & 0 & 0 & 0 & 0 & 0 & 0 & \frac{1}{2} \end{pmatrix} = -S_2^z, \tag{A9}$$

$$s_3^z = \begin{pmatrix} -\frac{\left(\sqrt{2}u+v\right)^2}{6} & 0 & \frac{u-\sqrt{2}v}{2\sqrt{3}} & 0 & 0 & \frac{-\sqrt{2}u^2+uv+\sqrt{2}v^2}{6} & 0 & 0 \\ 0 & \frac{1}{3} & 0 & -\frac{1}{2\sqrt{3}} & 0 & 0 & \frac{1}{3\sqrt{2}} & 0 \\ \frac{u-\sqrt{2}v}{2\sqrt{3}} & 0 & 0 & 0 & 0 & -\frac{\sqrt{2}u+v}{2\sqrt{3}} & 0 & 0 \\ 0 & -\frac{1}{3\sqrt{2}} & 0 & 0 & 0 & 0 & \frac{1}{\sqrt{6}} & 0 \\ 0 & 0 & 0 & 0 & -\frac{1}{2} & 0 & 0 & 0 \\ \frac{-\sqrt{2}u^2+uv+\sqrt{2}v^2}{6} & 0 & -\frac{\sqrt{2}u+v}{2\sqrt{3}} & 0 & 0 & -\frac{\left(u-\sqrt{2}v\right)^2}{6} & 0 & 0 \\ 0 & \frac{1}{3\sqrt{2}} & 0 & \frac{1}{\sqrt{6}} & 0 & 0 & \frac{1}{6} & 0 \\ 0 & 0 & 0 & 0 & 0 & 0 & 0 & \frac{1}{2} \end{pmatrix} = -S_3^z. \tag{A10}$$

APPENDIX B: ESTIMATION OF THE COUPLING J' BETWEEN LADDERS

The effective, antiferromagnetic coupling J' between neighboring spin stripes described by three-leg ladders is induced by the charge stripes between the ladders, since an antiferromagnetic alignment of the spins on each side of the charge stripe enhances the mobility of the holes. To determine this coupling, we have exactly diagonalized 16 site clusters of itinerant spin-1/2 antiferromagnets described by the t–J model[3,4] with $J = 0.4t$, two holes, and periodic boundary conditions (PBCs), in which the spin stripes are localized. The Hamiltonian is given by

$$\hat{H}_{\text{t-J-B}} = -t \sum_{\langle i,j\rangle,\sigma} \mathrm{P_G}\left(c_{i,\sigma}^\dagger c_{j,\sigma}^\dagger + \text{H.c.}\right)\mathrm{P_G} + J \sum_{\langle i,j\rangle} \hat{\mathbf{S}}_i \hat{\mathbf{S}}_j + \sum_{i \in \text{shaded area}} B_i \hat{S}_i^z, \tag{B1}$$

where the first two sums extend over all nearest-neighbor pairs $\langle i,j\rangle$, and $B_i = \pm B$ denotes a staggered magnetic field, as

indicated by the signs in Fig. 14. The Gutzwiller projector P_G eliminates doubly occupied sites.

We compare the ground-state energies we obtain for clusters with unfrustrated PBCs shown in Fig. 14(a) with the ground-state energies we obtain for clusters with frustrated PBCs shown in Fig. 14(b), in which the 16-site unit cells on the right are shifted by one lattice spacing to the top. We then consider spin-only Heisenberg models of three-leg ladders, which consist of only the sites in the shaded areas in Figs. 14(a) and 14(b), subject to the same staggered field B_i, and couple them antiferromagnetically by J', as indicated. The Heisenberg models are described by

$$\hat{H}_{\text{J-B}} = \sum_{\langle i,j \rangle} J_{ij} \hat{\mathbf{S}}_i \hat{\mathbf{S}}_j + \sum_{i \in \text{shaded area}} B_i \hat{S}^z_i \,, \tag{B2}$$

where $J_{ij} = J$ for all nearest-neighbor links inside the shaded areas, but $J_{ij} = J'$ for nearest-neighbor links across the horizontal boundary lines between those areas. We again compare the ground-state energies for unfrustrated PBCs, where J' couples sites 10 and 1, 11 and 2, etc., for the three-leg ladders shown in the shaded areas in Fig. 14(a), with frustrated PBCs, where J' couples sites 11 and 1, 12 and 2, etc., as shown in Fig. 14(b). Finally, we determine J' such that the difference in the ground-state energies between frustrated and unfrustrated PBCs in the t–J clusters matches this difference in the spin-only ladder models.

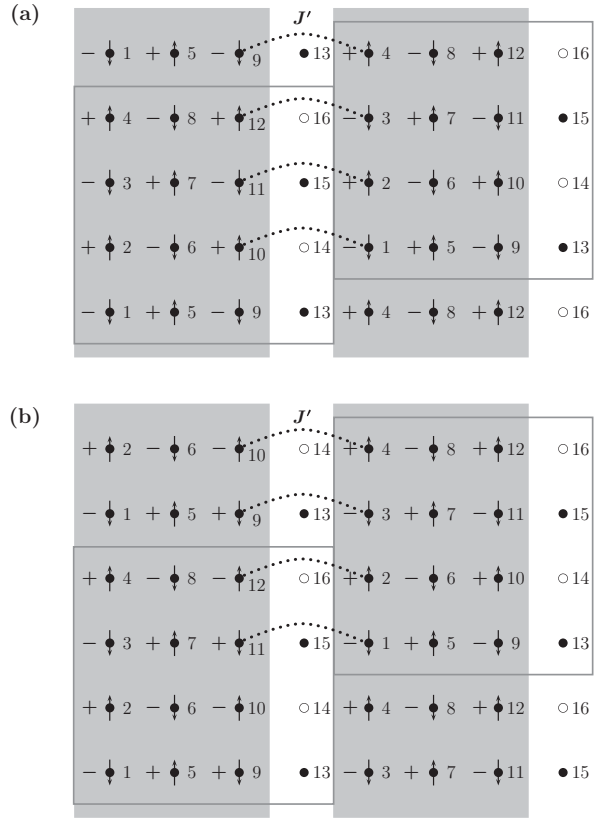

FIG. 14. Finite-size geometries with (a) unfrustrated and (b) frustrated periodic boundary conditions for site-centered stripe models. The spin stripes are localized by a staggered magnetic field B, as indicated by the signs in the grey shaded areas.

TABLE I. Ground state energies and expectation values of the staggered magnetic field term $\hat{H}_B = \sum B_i \hat{S}^z_i$, of $\hat{S}^z_i$, and of the electron densities $\hat{n}_i$ obtained by exactly diagonalization of the t–J model (B1) as well as the coupled Heisenberg ladders described by (B2) for the clusters shown in Fig. 14(a) and 14(b) for unfrustrated and frustrated periodic boundary conditions, respectively.

Site-centered stripe models			
PBCs as in	unfrustrated Fig. 14(a)	frustrated Fig. 14(b)	Δ
	t–J model with spin and charge stripes $t = 2.5$, $J = 1$, $B = 0.17$, $N = 16$, 2 holes		
E_{t-J-B}	−21.3409	−21.2405	0.1004
E_B	−0.5415		
$\langle \hat{S}^z_1 \rangle$	−0.3140		
$\langle \hat{S}^z_5 \rangle$	0.2411		
$\langle \hat{n}_1 \rangle$	0.9437		
$\langle \hat{n}_5 \rangle$	0.8781		
	three-leg Heisenberg ladder with coupling J' $J' = 0.071$, $J = 1$, $B = 0.17$, $N = 12$		
E_{J-B}	−8.0068	−7.9065	0.1003

With $B = 0.170J$ we obtain $J' = 0.071J$, as detailed in Table I. The value for \$B\$ is chosen self-consistently such that the mean value of the staggered magnetization we obtain for our spin wave theory in Appendix F,

$$\frac{1}{2}\left(-\langle \hat{s}^z_1 \rangle + \langle \hat{s}^z_2 \rangle\right) = 0.2903, \tag{B3}$$

matches the corresponding value in the t–J cluster shown in Fig. 14(a). For this cluster, however, there are two values for the staggered magnetization, depending on whether we consider the overall magnetization

$$\frac{1}{2}\left(-\langle \hat{S}^z_1 \rangle + \langle \hat{S}^z_5 \rangle\right) = 0.2775, \tag{B4}$$

or the magnetization on only those sites which are occupied by electrons (which differs since the holes are not strictly localized on the chain in between the shaded areas in Fig. 14(b)):

$$\frac{1}{2}\left(-\frac{\langle \hat{S}^z_1 \rangle}{\langle \hat{n}_1 \rangle} + \frac{\langle \hat{S}^z_5 \rangle}{\langle \hat{n}_5 \rangle}\right) = 0.3037. \tag{B5}$$

We assert that these two values constitute lower and upper bounds of what we would expect in a spin-only model, and chose B such that the spin wave theory gives the mean value of these bounds (this value is 0.2906).

For completeness, we also provide the details of the corresponding calculation for the effective coupling J' between bond-centered stripes modelled by two-leg ladders, in Table II. The calculation differs only in that we now use the finite size clusters depicted in Figs. 15(a) and (b). The value of the staggered magnetic field $B = 0.225$ is chosen such that the staggered magnetic field energy E_B described by the last term in (B1) is equal to the value we obtained for the three-leg ladder model listed in see Table I. We obtain a ferromagnetic coupling

TABLE II. Ground-state energies and the expectation value of the staggered magnetic field term $\hat{H}_B = \sum B_i \hat{S}^z_i$ obtained by exactly diagonalization of the t–J model (B1) as well as the coupled Heisenberg ladders described by (B2) for the clusters shown in Figs. 15(a) and (b) for unfrustrated and frustrated periodic boundary conditions, respectively.

Bond-centered stripe models			
PBCs	unfrustrated	frustrated	Δ
as in	Fig. 15(a)	Fig. 15(b)	
	t–J model with spin and charge stripes		
	$t = 2.5$, $J = 1$, $B = 0.225$, $N = 16$, 2 holes		
E_{t-J-B}	-21.3428	-21.2526	0.0902
E_B	-0.5395		
	two-leg Heisenberg ladder with coupling J'		
	$J' = -0.051$, $J = 1$, $B = 0.225$, $N = 8$		
E_{J-B}	-5.1557	-5.0655	0.0902

$J' = -0.051J$. This value is not large enough to close the spin gap $\Delta \approx J/2$ of the the individual two-leg ladders, and hence precludes a description of bond-centered stripes in terms of spin-only models of coupled two-leg ladders.[36]

It should be born in mind that the values we obtain here are only estimates, as it is impossible to calculate a precise value for a coupling between spin-only models of stripes, as these constitute a rather crude approximation themselves. We are confident, however, that the coupling for three-leg ladders modeling site-centered stripes is between $J' = 0.05J$ and $J' = 0.1J$, and that the absolute value of the coupling between two-leg ladders describing bond-centered stripes is significantly smaller than this coupling.

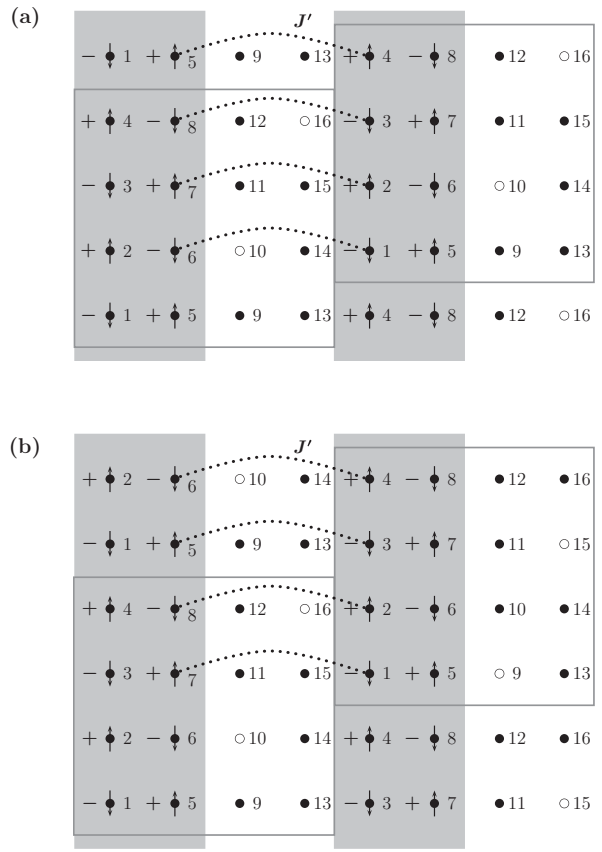

FIG. 15. Finite size geometries with (a) unfrustrated and (b) frustrated periodic boundary conditions for bond-centered stripe models. The spin stripes are localized by a staggered magnetic field B as indicated by the signs in the gray shaded areas.

APPENDIX C: ANALYSIS OF $\tilde{E}_0$, $\hat{H}_{a0}$, $\hat{H}_{c0}$, $\hat{H}_{a1}$, AND $\hat{H}_{c2}$

In this appendix, we expand and analyze the terms in the Hamiltonian (26) which have no influence on the low energy spectrum in this appendix. These terms, however, are required for evaluations of the ground-state energy.

1. The bare ground-state energy $\tilde{E}_0$

The bare ground-state energy $\tilde{E}_0$ accounts for the constant terms in the Hamiltonian (17). It is given by $\tilde{E}_0 = \sum_{\boldsymbol{k}} 2\tilde{\varepsilon}_0 = N\tilde{\varepsilon}_0$ with

$$\begin{aligned}\tilde{\varepsilon}_0 &= \frac{1}{2} - \frac{3}{2}u^2 + J\sum_{\alpha=1}^{3} s^z_{\alpha,11}S^z_{\alpha,11} + J' s^z_{3,11}S^z_{1,11} \\ &= -1.45842. \end{aligned} \tag{C1}$$

2. Evaluation of the spectrum of $\hat{H}_{a0}$

The term $\hat{H}_{a0}$ is given by

$$\begin{aligned}\hat{H}_{a0} = \sum_k \Big[&\varepsilon_{a0}\big(a^\dagger_{0,k}a_{0,k} + A^\dagger_{0,k}A_{0,k}\big) \\ &+ \xi_{a0,k}\big(a^\dagger_{0,k} + a_{0,k}\big)\big(A^\dagger_{0,k} + A_{0,k}\big)\Big],\end{aligned} \tag{C2}$$

with

$$\begin{aligned}\varepsilon_{a0} &= -\frac{1}{2} + \frac{3}{2}u^2 - 2J\sum_{\alpha=1}^{3} s^z_{\alpha,11}S^z_{\alpha,11} - 2J' s^z_{3,11}S^z_{1,11}, \\ \xi_{a0,k} &= J'\cos(4k_x)\, s^z_{3,13}S^z_{1,13} + J\cos k_y \sum_{\alpha=1}^{3} s^z_{\alpha,13}S^z_{\alpha,13}.\end{aligned} \tag{C3}$$

To a reasonable approximation, we obtain low energy modes described by $\hat{H}_{a0}$ by diagonalizing (C2) at each point in $\boldsymbol{k}$ space in the reduced Hilbert space spanned by

$$|\tilde{0}\rangle,\ a^\dagger_0|\tilde{0}\rangle,\ A^\dagger_0|\tilde{0}\rangle, \text{ and } a^\dagger_0 A^\dagger_0|\tilde{0}\rangle,$$

where

$$|\tilde{0}\rangle \equiv \prod_{i\in\mathcal{A}} |\tilde{b}_{-1/2}\rangle_i \cdot \prod_{j\in\mathcal{B}} |\tilde{b}_{1/2}\rangle_j \tag{C4}$$

is the bare vacuum unrenormalized by spin wave theory. This yields two almost dispersionless modes

$$(\omega_{a0,k})_{1/2} = \sqrt{\varepsilon^2_{a0} + \xi^2_{a0,k}} \pm \xi_{a0,k}, \tag{C5}$$

with energies of about $\varepsilon_{a0} = 2.07$, or 290 meV if we assume $J_{\text{exp.}} = 140$ meV. Cuts of the dispersions of these two modes

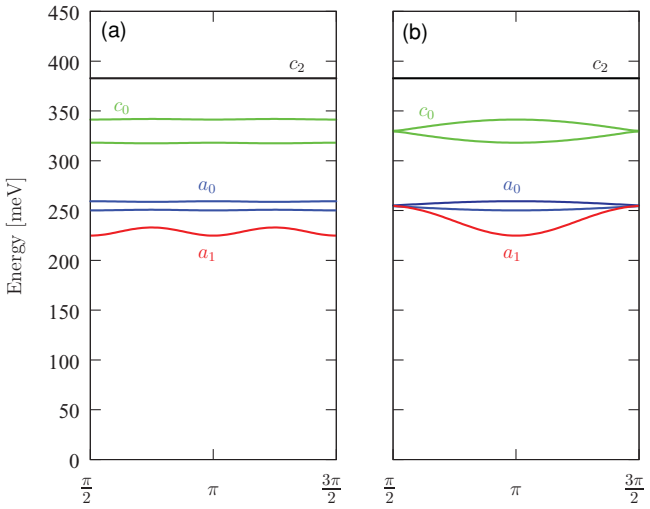

FIG. 16. (Color online) Modes described by $\hat{H}_{a0}$ (blue), $\hat{H}_{c0}$ (green), $\hat{H}_{a1}$ (red), $\hat{H}_{c-2}$ (black) plotted as cuts (a) along (k_x, π) and (b) along (π, k_y) using $J_{\rm exp} = 140$ meV.

are shown in blue (color online) in Fig. 16. $\hat{H}_{a0}$ also gives rise to a contribution

$$E_{a0} = \sum_k \left(\varepsilon_{a0} - \sqrt{\varepsilon_{a0}^2 + \xi_{a0,k}^2}\right) = -0.00008\, N \quad \text{(C6)}$$

to the ground-state energy. (Here N denotes the number of rungs, which implies that the sum extends over $\frac{N}{2}$ values for $\boldsymbol{k}$.)

3. Evaluation of the spectrum of $\hat{H}_{c0}$

A similar analysis of

$$\hat{H}_{c0} = \sum_k \Big[\varepsilon_{c0}\big(c_{0,k}^\dagger c_{0,k} + C_{0,k}^\dagger C_{0,k}\big) + \xi_{c0,k}\big(c_{0,k}^\dagger + c_{0,k}\big)\big(C_{0,k}^\dagger + C_{0,k}\big)\Big], \quad \text{(C7)}$$

with

$$\varepsilon_{c0} = \tfrac{3}{2}\left(u^2 - v^2\right) + 2J\sum_{\alpha=1}^3 s_{\alpha,11}^z (S_{\alpha,66}^z - S_{\alpha,11}^z) + 2J' s_{3,11}^z (S_{1,66}^z - S_{1,11}^z), \quad \text{(C8)}$$

$$\xi_{c0,k} = J'\cos(4k_x)\, s_{3,16}^z S_{1,16}^z + J\cos k_y \sum_{\alpha=1}^3 s_{\alpha,16}^z S_{\alpha,16}^z, \quad \text{(C9)}$$

yields two additional, almost dispersionless modes

$$(\omega_{c0,k})_{1/2} = \sqrt{\varepsilon_{c0}^2 + \xi_{c0,k}^2} \pm \xi_{c0,k}, \quad \text{(C10)}$$

with energies of about $\varepsilon_{c0} = 2.71$, or 380 meV, which is shown in green (color online) in Fig. 16. $\hat{H}_{c0}$ also gives rise to a contribution

$$E_{c0} = \sum_k \left(\varepsilon_{c0} - \sqrt{\varepsilon_{c0}^2 + \xi_{c0,k}^2}\right) = -0.00048\, N \quad \text{(C11)}$$

to the ground-state energy.

4. Evaluation of the spectrum of $\hat{H}_{a1}$

The term

$$\hat{H}_{a1} = \sum_k \Big[\varepsilon_{a1}\big(a_{1,k}^\dagger a_{1,k} + A_{-1,k}^\dagger A_{-1,k}\big) + \xi_{a1,k}\big(a_{1,k}^\dagger A_{-1,k}^\dagger + a_{1,k} A_{-1,k}\big)\Big], \quad \text{(C12)}$$

with $\varepsilon_{a1} = \varepsilon_{a0}$ as given in (C3) and

$$\xi_{a1,k} = J'\cos(4k_x) s_{3,41}^+ S_{1,41}^- + J\cos k_y \sum_{\alpha=1}^3 s_{\alpha,41}^+ S_{\alpha,41}^-, \quad \text{(C13)}$$

can be diagonalized by a Bogoliubov transformation. We obtain

$$\hat{H}_{a1} = \sum_k \left[\omega_{a1,k}\big(\alpha_{1,k}^\dagger \alpha_{1,k} + \alpha_{2,k}^\dagger \alpha_{2,k}\big) + \omega_{a1,k} - \varepsilon_{a1}\right] \quad \text{(C14)}$$

with

$$\omega_{a1,k} = \sqrt{\varepsilon_{a1}^2 - \xi_{a1,k}^2}. \quad \text{(C15)}$$

It yields a twofold degenerate, weakly dispersing mode with an energy of about 1.95, or 273 meV, which is shown in red (color online) in Fig. 16, as well as a contribution

$$E_{a1} = \sum_k \left(\omega_{a1,k} - \varepsilon_{a1}\right) = -0.05363\, N \quad \text{(C16)}$$

to the ground-state energy.

5. Evaluation of the spectrum of $\hat{H}_{c2}$

Finally,

$$\hat{H}_{c2} = \sum_k \omega_{c2}\big(c_{2,k}^\dagger c_{2,k} + C_{-2,k}^\dagger C_{-2,k}\big) \quad \text{(C17)}$$

with

$$\omega_{c2} = \frac{3}{2}u^2 + 2J\sum_{\alpha=1}^3 s_{\alpha,11}^z (S_{\alpha,88}^z - S_{\alpha,11}^z) + 2J' s_{3,11}^z (S_{1,88}^z - S_{1,11}^z), \quad \text{(C18)}$$

describes a twofold degenerate, completely dispersionless mode with an energy of $\omega_{c2} = 3.12$, or 436 meV.

APPENDIX D: GROUND-STATE ENERGY

To evaluate the ground state energy E_0, we collect the contributions from (C1), (C6), (C11), (C16), and (44). This yields

$$E_0 = -1.73378\, N, \quad \text{(D1)}$$

where N is the number of rungs. This number is in good agreement with what we would expect from the results of exact diagonalizations of

$$\hat{H}_J = \sum_{\langle i,j\rangle} J_{ij}\hat{\mathbf{S}}_i \hat{\mathbf{S}}_j \quad \text{(D2)}$$

for small clusters of 12, 18, and 24 sites with unfrustrated boundary conditions, as shown for $N = 4$ rungs by the shaded

areas in Fig. 14(a). Specifically, we obtain $E_0 = -1.827\,N$ for a cluster with $N = 8$ rungs, $J' = 0.07$, and unfrustrated boundary conditions with a shift of three lattice spacings. If we compare the nearest-neighbor spin-spin correlation we obtain from exactly diagonalizing the same 24-site cluster with $J' = 1$, $\langle \hat{\boldsymbol{S}}_i \hat{\boldsymbol{S}}_j \rangle = -0.343$, to the the value predicted by standard two-dimensional linear spin wave theory[42], $\langle \hat{\boldsymbol{S}}_i \hat{\boldsymbol{S}}_j \rangle = -0.329$, we are led to estimate that the bond operator spin wave theory developed here should yield a number around

$$E_0 = -1.827\,N \cdot \frac{-0.329}{-0.3432} = -1.751\,N. \tag{D3}$$

This differs only by 1% from (D1).

APPENDIX E: MATRIX ELEMENTS

The dynamical structure factor measured in neutron scattering is given by

$$\chi^{+-}(k,\omega) = \sum_n |\langle 0|\hat{S}^+_k|n\rangle|^2 \delta(\omega - \omega_n), \tag{E1}$$

where $|0\rangle$ is the ground state and the sum extends over all excited states $|n\rangle$ with energy ω_n, and

$$\hat{S}^+_k = \sum_l e^{-ik\boldsymbol{r}_l} \hat{S}^+_l \tag{E2}$$

is the Fourier transform of the spin raising operator $\hat{S}_l$ at lattice site l with respect to original lattice, i.e., the sum runs over all lattice sites. This implies

$$\boldsymbol{r}_{i,\alpha} = \boldsymbol{R}_i + \begin{pmatrix} \alpha - 2 \\ 0 \end{pmatrix}, \tag{E3}$$

$$\boldsymbol{r}_{j,\alpha} = \boldsymbol{R}_j + \begin{pmatrix} \alpha - 2 \\ 0 \end{pmatrix}, \tag{E4}$$

with $\boldsymbol{R}_i$ and $\boldsymbol{R}_j$ as indicated in Fig. 7 for sublattices A and B, respectively. In analogy to Fourier transforms of the bosonic creation and annihilation operators (23) and (24), we further Fourier transforms of the spin operators with respect to the rung sublattices $\mathcal{A}$ and $\mathcal{B}$ according to

$$\hat{s}^+_{k,\alpha} = \sqrt{\frac{2}{N}} \sum_{i\in\mathcal{A}} e^{-ik\boldsymbol{R}_i} \hat{s}^+_{i,\alpha}, \tag{E5}$$

$$\hat{S}^+_{k,\alpha} = \sqrt{\frac{2}{N}} \sum_{j\in\mathcal{B}} e^{-ik\boldsymbol{R}_j} \hat{S}^+_{j,\alpha}, \tag{E6}$$

and express the operator (E2) in terms of them:

$$\begin{aligned} \hat{S}^+_k &= \sqrt{\frac{2}{N}} \left\{ \sum_{i\in\mathcal{A}} \sum_\alpha e^{-ik\boldsymbol{r}_{i,\alpha}} \hat{s}^+_{i,\alpha} + \sum_{j\in\mathcal{B}} \sum_\alpha e^{-ik\boldsymbol{r}_{j,\alpha}} \hat{S}^+_{j,\alpha} \right\} \\ &= \sum_\alpha e^{-ik_x(\alpha-2)} s^+_{k,\alpha} + \sum_\alpha e^{-ik_x(\alpha-2)} S^+_{k,\alpha} \\ &= \sum_\alpha e^{-ik_x(\alpha-2)} \left(\hat{s}^+_{k,\alpha} + \hat{S}^+_{k,\alpha}\right). \end{aligned} \tag{E7}$$

As we are interested only in the contribution of the low-energy mode $\omega_{k,1}$ to $\chi^{+-}(k,\omega)$, the only matrix element we need to evaluate is

$$\left|\langle 0|\hat{S}^+_k|\gamma_{1,k}\rangle\right|^2 = \left|\langle 0|\hat{S}^+_k \gamma^\dagger_{1,k}|0\rangle\right|^2 \tag{E8}$$

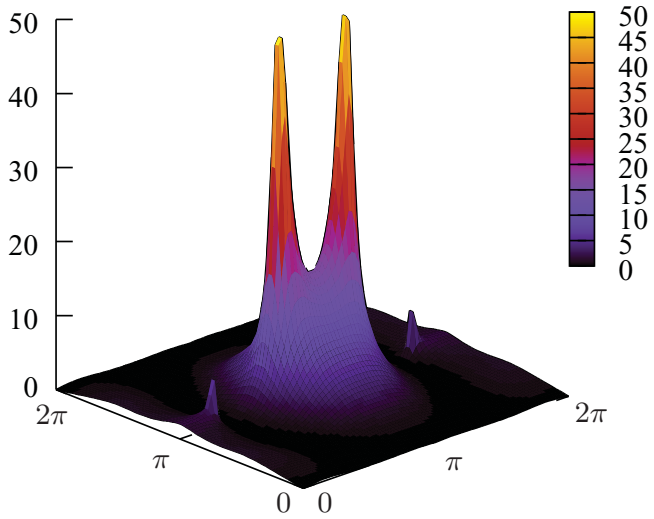

FIG. 17. (Color online) Numerical evaluation of the matrix elements $|\langle 0|\hat{S}^+_{\boldsymbol{k}}|\gamma_{1,\boldsymbol{k}}\rangle|^2$ for the entire Brillouin zone $\boldsymbol{k} \in [0,2\pi] \times [0,2\pi]$. Note the strong enhancement aground the antiferromagnetic ordering wave vectors $\boldsymbol{k} = (\pi \pm \pi/4, \pi)$.

for all values of $\boldsymbol{k}$. [The second low-energy mode $\omega_{\boldsymbol{k},2}$, which is degenerate with the first, does not contribute to (E8) and hence to $\chi^{+-}(\boldsymbol{k},\omega)$, but instead yields a contribution to $\chi^{-+}(\boldsymbol{k},\omega)$ which is identical to the one we calculate below.] Keeping only terms which contribute to this mode and are linear in the expansion (14) of $\hat{s}^+_\alpha$, we obtain for sublattice $\mathcal{A}$

$$\hat{s}^+_\alpha = s^+_{\alpha,21} b^\dagger_1 + s^+_{\alpha,71} c^\dagger_1 + s^+_{\alpha,15} c_{-1}$$

or in Fourier space with (E5), (23), and (28)

$$\begin{aligned} \hat{s}^+_{k,\alpha} &= s^+_{\alpha,21} b^\dagger_{1,k} + s^+_{\alpha,71} c^\dagger_{1,k} + s^+_{\alpha,15} c_{-1,-k} \\ &= \left(0, s^+_{\alpha,21}, 0, s^+_{\alpha,71}, 0, s^+_{\alpha,15}\right) \cdot \Psi_k \end{aligned} \tag{E9}$$

and similarly with (16) and (24) for $\mathcal{B}$

$$\begin{aligned} \hat{S}^+_{k,\alpha} &= S^+_{\alpha,12} B_{-1,k} + S^+_{\alpha,17} C_{-1,k} + S^+_{\alpha,51} C^\dagger_{1,-k} \\ &= \left(S^+_{\alpha,12}, 0, S^+_{\alpha,17}, 0, S^+_{\alpha,51}, 0\right) \cdot \Psi_k. \end{aligned} \tag{E10}$$

We then use $\Psi_{\boldsymbol{k}} = M_{\boldsymbol{k}} \Gamma_{\boldsymbol{k}}$ and (42) to express $\hat{s}^+_{\boldsymbol{k},\alpha}$ and $\hat{S}^+_{\boldsymbol{k},\alpha}$ in terms of $\gamma_{i,\boldsymbol{k}}$ and $\gamma^\dagger_{i,\boldsymbol{k}}$, recall $S^+_{\alpha,ji} = s^+_{\alpha,ij}$, and finally obtain

$$\begin{aligned} \left|\langle 0|\hat{S}^+_k|\gamma_{1,k}\rangle\right|^2 = \Bigg| \sum_{\alpha=1}^{3} e^{-ik_x(\alpha-2)} \big\{ & s^+_{\alpha,21}(M_{k,11} + M_{k,21}) \\ & + s^+_{\alpha,71}(M_{k,31} + M_{k,41}) \\ & + s^+_{\alpha,15}(M_{k,51} + M_{k,61}) \big\} \Bigg|^2 . \end{aligned} \tag{E11}$$

The result is plotted in Fig. 17. Note that $\chi^{zz}(\boldsymbol{k},\omega) = 0$ as there is no term linear in $b^\dagger_1$, $c^\dagger_1$, or c_{-1} in the expansion (14) for $\hat{s}^z_\alpha$.

APPENDIX F: STAGGERED MAGNETIZATION

The staggered magnetizations on the outer and inner chains of our three-leg ladders, $\langle \hat{s}_1^z \rangle = \langle \hat{s}_3^z \rangle = -\langle \hat{S}_1^z \rangle = -\langle \hat{S}_3^z \rangle$ and $\langle \hat{s}_2^z \rangle = -\langle \hat{S}_2^z \rangle$, respectively, are given in by the the bare values $s^z_{\alpha,11} = -S^z_{\alpha,11}$ with $\alpha = 1,2,3$ minus corrections from the individual terms in the Hamiltonian (26). From (A8)–(A10) with (22), we obtain for the bare values

$$\langle \hat{s}_1^z \rangle_{\text{bare}} = s^z_{1,11} = -0.4633, \tag{F1}$$

$$\langle \hat{s}_2^z \rangle_{\text{bare}} = s^z_{2,11} = 0.4265. \tag{F2}$$

We expect that the largest corrections arise from $\hat{H}_{b1,c1,c-1}$, as this part contains the only low energy mode of the theory. The for this part relevant terms in the expansion (14) for $\hat{s}^z_\alpha$ are

$$\begin{aligned} & b_1^\dagger b_1 \left(s^z_{\alpha,22} - s^z_{\alpha,11}\right) + c_1^\dagger c_1 \left(s^z_{\alpha,77} - s^z_{\alpha,11}\right) \\ & \quad + c_{-1}^\dagger c_{-1} \left(s^z_{\alpha,55} - s^z_{\alpha,11}\right) \\ & \quad + \left(b_1^\dagger c_1 + c_1^\dagger b_1\right) s^z_{\alpha,27}. \end{aligned}$$

For convenience, we define

$$\begin{aligned} \rho_{\alpha,1} &= \left(s^z_{\alpha,22} - s^z_{\alpha,11}\right), \\ \rho_{\alpha,2} &= \left(s^z_{\alpha,77} - s^z_{\alpha,11}\right), \\ \rho_{\alpha,3} &= \left(s^z_{\alpha,55} - s^z_{\alpha,11}\right). \end{aligned} \tag{F3}$$

and express the operators $b_1, c_1, c_{-1}^\dagger$ as well as their Hermitian conjugates via $\Psi = M\Gamma$ through the γ operators [see (28), (34), and (42) above]. Using $\gamma_j |0\rangle = \langle 0|\gamma_j^\dagger = 0$ and $\langle 0|\gamma_i \gamma_j^\dagger|0\rangle = \delta_{ij}$, we obtain for the corrections from $\hat{H}_{b1,c1,c-1}$

$$\begin{aligned} \langle \hat{s}^z_\alpha \rangle_{\hat{H}_{b1,c1,c-1}} = \frac{2}{N} \sum_k \Big\{ & \Big[\rho_{\alpha,1} M_{k,21} M^T_{k,12} + \rho_{\alpha,2} M_{k,41} M^T_{k,14} + \rho_{\alpha,3} M_{k,62} M^T_{k,26} + s^z_{\alpha,27} \left(M_{k,21} M^T_{k,14} + M_{k,41} M^T_{k,12} \right) \Big] \\ & + \Big[\rho_{\alpha,1} M_{k,23} M^T_{k,32} + \rho_{\alpha,2} M_{k,43} M^T_{k,34} + \rho_{\alpha,3} M_{k,64} M^T_{k,46} + s^z_{\alpha,27} \left(M_{k,23} M^T_{k,34} + M_{k,43} M^T_{k,32} \right) \Big] \\ & + \Big[\rho_{\alpha,1} M_{k,26} M^T_{k,62} + \rho_{\alpha,2} M_{k,46} M^T_{k,64} + \rho_{\alpha,3} M_{k,65} M^T_{k,56} + s^z_{\alpha,27} \left(M_{k,26} M^T_{k,64} + M_{k,46} M^T_{k,62} \right) \Big] \Big\}. \end{aligned}$$

In this sum, the terms in the first pair of square brackets originate from the low-energy eigenmodes γ_1, γ_2 in the energy range from 0 to about 190 meV in Fig. 9, the terms in the second pair originate form γ_3, γ_4 at about 290 meV, and the terms in the third pair originate from γ_5, γ_6 at about 460 meV. Evaluation yields

$$\begin{aligned} \langle \hat{s}_1^z \rangle_{\hat{H}_{b1,c1,c-1}} &= 0.1752 + 0.0018 + 0.0003 \\ &= 0.1773, \end{aligned} \tag{F4}$$

$$\begin{aligned} \langle \hat{s}_2^z \rangle_{\hat{H}_{b1,c1,c-1}} &= -0.0864 - 0.0210 - 0.0001 \\ &= -0.1075, \end{aligned} \tag{F5}$$

for the outer and inner chains, respectively. As expected, the low energy mode we compare to the experiment[15] yields the dominant contribution.

The corrections arising from $\hat{H}_{a1}$ are evaluated in complete analogy. The Bogoliubov transformation $\Psi_a = M_a \Gamma_a$ with $\Psi_a \equiv (A_{-1}, a_1^\dagger)^T$ is now only two-dimensional, and the only contribution comes from the term $-s^z_{\alpha,11} a_1^\dagger a_1$ in (14):

$$\langle \hat{s}^z_\alpha \rangle_{\hat{H}_{a1}} = -\frac{2}{N} \sum_k s^z_{\alpha,11} M_{a,k,21} M^T_{a,k,12}. \tag{F6}$$

Evaluation yields

$$\langle \hat{s}_1^z \rangle_{\hat{H}_{a1}} = 0.0127, \tag{F7}$$

$$\langle \hat{s}_2^z \rangle_{\hat{H}_{a1}} = -0.0117. \tag{F8}$$

Finally, $\hat{H}_{a0}$ and $\hat{H}_{c0}$ give rise to corrections

$$\langle \hat{s}^z_\alpha \rangle_{\hat{H}_{a0}} = \left(-s^z_{\alpha,11}\right) \frac{2}{N} \sum_k \frac{1}{N^2_{a0,k}}, \tag{F9}$$

$$\langle \hat{s}^z_\alpha \rangle_{\hat{H}_{c0}} = \left(s_{\alpha,66} - s^z_{\alpha,11}\right) \frac{2}{N} \sum_k \frac{1}{N^2_{c0,k}}, \tag{F10}$$

where

$$N^2_{ao,k} = \left(\frac{\epsilon_{a0} + \sqrt{\epsilon^2_{a0} + \xi^2_{a0,k}}}{\xi_{a0,k}} \right)^2 + 1, \tag{F11}$$

$$N^2_{ao,k} = \left(\frac{\epsilon_{c0} + \sqrt{\epsilon^2_{c0} + \xi^2_{c0,k}}}{\xi_{c0,k}} \right)^2 + 1 \tag{F12}$$

with ϵ_{a0} and $\xi_{a0,\boldsymbol{k}}$ as given in (C3) and (C4) and ϵ_{c0} and $\xi_{c0,\boldsymbol{k}}$ as given in (C8) and (C9). Evaluation yields

$$\langle \hat{s}_1^z \rangle_{\hat{H}_{a0}} + \langle \hat{s}_1^z \rangle_{\hat{H}_{c0}} = 0.0001, \tag{F13}$$

$$\langle \hat{s}_2^z \rangle_{\hat{H}_{a0}} + \langle \hat{s}_2^z \rangle_{\hat{H}_{c0}} = -0.0001, \tag{F14}$$

i.e., negligibly small contributions.

Summing up (F1), (F4), (F7), (F13), and (F2), (F5), (F8), (F14), we obtain

$$\langle \hat{s}_1^z \rangle = -0.2732, \tag{F15}$$

$$\langle \hat{s}_2^z \rangle = 0.3072 \tag{F16}$$

for the staggered magnetizations on the outer and inner chains of the three-leg ladders, respectively.

[1] J. Zaanen *et al*., Nature Phys. **2**, 138 (2006).
[2] J. Orenstein and A. J. Millis, Science **288**, 468 (2000).
[3] F. C. Zhang and T. M. Rice, Phys. Rev. B **37**, 3759 (1988).
[4] H. Eskes and G. A. Sawatzky, Phys. Rev. Lett. **61**, 1415 (1988).
[5] H. F. Fong, B. Keimer, P. W. Anderson, D. Reznik, F. Doğan, and I. A. Aksay, Phys. Rev. Lett. **75**, 316 (1995).
[6] P. Bourges, Y. Sidis, H. F. Fong, L. P. Regnault, J. Bossy, A. Ivanov, and B. Keimer, Science **288**, 1234 (2000).
[7] J. Zaanen and O. Gunnarsson, Phys. Rev. B **40**, 7391 (1989).
[8] M. Kato, K. Machida, H. Nakanishi, and M. Fujita, J. Phys. Soc. Jpn. **59**, 1047 (1990).
[9] J. M. Tranquada, B. J. Sternlieb, J. D. Axe, Y. Nakamura, and S. Uchida, Nature (London) **375**, 561 (1995).
[10] V. J. Emery, S. Kivelson, and J. Tranquada, Proc. Natl. Acad. Sci. U.S.A. **96**, 8814 (1999).
[11] J. Zaanen, O. Y. Osman, H. V. Kruis, Z. Nussinov, and J. Tworzydło, Phil. Mag. B **81**, 1485 (2001).
[12] H. A. Mook, P. Dai, and F. Doğan, Phys. Rev. Lett. **88**, 097004 (2002).
[13] S. A. Kivelson, I. P. Bindloss, E. Fradkin, V. Oganesyan, J. M. Tranquada, A. Kapitulnik, and C. Howald, Rev. Mod. Phys. **75**, 1201 (2003).
[14] E. Berg, E. Fradkin, S. A. Kivelson, and J. Tranquada, New J. Phys. **11**, 115004 (2009).
[15] J. Tranquada, H. Woo, T. Perring, H. Goka, G. Gu, G. Xu, M. Fujita, and K. Yamada, Nature (London) **429**, 534 (2004).
[16] B. Fauqué, Y. Sidis, L. Capogna, A. Ivanov, K. Hradil, C. Ulrich, A. I. Rykov, B. Keimer, and P. Bourges, Phys. Rev. B **76**, 214512 (2007).
[17] E. Dagotto and T. M. Rice, Science **271**, 618 (1996).
[18] D. G. Shelton, A. A. Nersesyan, and A. M. Tsvelik, Phys. Rev. B **53**, 8521 (1996).
[19] M. Greiter, Phys. Rev. B **66**, 054505 (2002).
[20] G. Xu, J. M. Tranquada, T. G. Perring, G. D. Gu, M. Fujita, and K. Yamada, Phys. Rev. B **76**, 014508 (2007).
[21] V. Hinkov, S. Pailhes, P. Bourges, Y. Sidis, A. Ivanov, A. Kulakov, C. T. Lin, D. P. Chen, C. Bernhard, and B. Keimer, Nature (London) **430**, 650 (2004).
[22] V. Hinkov, P. Bourges, S. Pailhès, Y. Sidis, A. Ivanov, C. D. Frost, T. G. Perring, C. T. Lin, D. P. Chen, and B. Keimer, Nature Physics **3**, 780 (2007).
[23] M. Vojta and T. Ulbricht, Phys. Rev. Lett. **93**, 127002 (2004).
[24] G. S. Uhrig, K. P. Schmidt, and M. Grüninger, Phys. Rev. Lett **93**, 267003 (2004).
[25] V. I. Anisimov, M. A. Korotin, A. S. Mylnikova, A. V. Kozhevnikov, D. M. Korotin, and J. Lorenzana, Phys. Rev. B **70**, 172501 (2004).
[26] S. Sachdev and R. N. Bhatt, Phys. Rev. B **41**, 9323 (1990).
[27] F. Krüger and S. Scheidl, Phys. Rev. B **67**, 134512 (2003).
[28] R. Eder, Phys. Rev. B **57**, 12832 (1998).
[29] S. Gopalan, T. M. Rice, and M. Sigrist, Phys. Rev. B **49**, 8901 (1994).
[30] J. Tworzydło, O. Y. Osman, C. N. A. van Duin, and J. Zaanen, Phys. Rev. B **59**, 115 (1999).
[31] S. Dalosto and J. Riera, Phys. Rev. B **62**, 928 (2000).
[32] T. S. Nunner, P. Brune, T. Kopp, M. Windt, and M. Grüninger, Phys. Rev. B **66**, 180404(R) (2002).
[33] G. Seibold and J. Lorenzana, Phys. Rev. Lett. **94**, 107006 (2005).
[34] G. Seibold and J. Lorenzana, Phys. Rev. B **73**, 144515 (2006).
[35] R. M. Konik, F. H. L. Essler, and A. M. Tsvelik, Phys. Rev. B **78**, 214509 (2008).
[36] M. Greiter and H. Schmidt, Phys. Rev. B **82**, 144512 (2010).
[37] D. X. Yao, E. W. Carlson, and D. K. Campbell, Phys. Rev. Lett. **97**, 017003 (2006).
[38] S. Sachdev, Phys. Rev. B **45**, 12377 (1992).
[39] M. Greiter, Phys. Rev. B **65**, 134443 (2002).
[40] T. M. Rice, S. Haas, M. Sigrist, and F.-C. Zhang, Phys. Rev. B **56**, 14655 (1997).
[41] M. Greiter, Ann. Phys. (NY) **325**, 1349 (2010).
[42] P. W. Anderson, Phys. Rev. **86**, 694 (1952).